RSC Advances

REVIEW

View Article Online
View Journal | View Issue

Cite this: *RSC Adv.*, 2023, **13**, 20889

Progress in photocatalytic CO_2 reduction based on single-atom catalysts

Wanyu Hu,[a] Haiyue Yang *[ab] and Chengyu Wang *[ab]

Reduced CO_2 emissions, conversion, and reuse are critical steps toward carbon peaking and carbon neutrality. Converting CO_2 into high-value carbon-containing compounds or fuels may effectively address the energy shortage and environmental issues, which is consistent with the notion of sustainable development. Photocatalytic CO_2 reduction processes have become one of the research focuses, where single-atom catalysts have demonstrated significant benefits owing to their excellent percentage of atom utilization. However, among the crucial challenges confronting contemporary research is the production of efficient, low-cost, and durable photocatalysts. In this paper, we offer a comprehensive overview of the study growth on single-atom catalysts for photocatalytic CO_2 reduction reactions, describe several techniques for preparing single-atom catalysts, and discuss the advantages and disadvantages of single-atom catalysts and present the study findings of three single-atom photocatalysts with TiO_2, g-C_3N_4 and MOFs materials as carriers based on the interaction between single atoms and carriers, and finally provide an outlook on the innovation of photocatalytic CO_2 reduction reactions.

Received 24th May 2023
Accepted 3rd July 2023

DOI: 10.1039/d3ra03462c

rsc.li/rsc-advances

Introduction

As mankind enters the era of the industrial revolution, raw fossil materials are widely used in production and life as the main energy materials, causing a sharp rise in emissions of CO_2.[1] CO_2 as a typical greenhouse gas, will increase surface temperature by 1.5 to 4.5 °C for every 1-fold increase in concentration.[2] As a result of modernization, significant CO_2 emissions have brought severe ecological and environmental problems, for instance, global warming, the greenhouse effect, glacier and permafrost melting, sea level rising, *etc.*,[2] which are threatening the survival and living environment of human beings at all times and posing significant obstacles to the future sustainable growth of human civilization. Countries are always paying attention to the global climate problem, and China has shown great concern and determination in this regard. China suggested during the 75th UN General Assembly in September 2020 that "China should strive to reach a peak in carbon dioxide emissions by 2030 and work towards achieving carbon neutrality by 2060".[4]

On the other hand, reliable energy and chemical sources are crucial to our contemporary lifestyles, which are necessary for mobility, wealth, and daily comfort.[3–5] We now need to look for sustainable and environmentally acceptable alternative resources along with the depletion of resources derived from fossil fuels as well as their significant influence on environmental damage.[6] There is now widespread agreement that CO_2 emissions should be successfully decreased[7] *via* renewable energy conversion techniques and possibly provide high-value carbon-containing compounds or fuels.[8] Therefore, scientists put forward the concept of artificial catalytic light energy conversion. Through direct solar energy collecting, artificial converting photocatalytic energy is a practical solution to the problems of environmental protection and energy security[9] because of its cleanliness, inexhaustibility, efficiency, and cost-effectiveness.[10] To make use of unlimited and freely available solar energy, artificial photocatalytic energy conversion delivers a further deployable and encouraging strategy that can combat the global energy crisis and cope with the extremely volatile climate by converting greenhouse gas CO_2 into high-value carbon-containing compounds and finally ending the carbon cycle.[11,12] As a result, CO_2 reduction reactions have attracted extensive attention from researchers across the country.[13] Solar-powered CO_2 conversion to fuel is an appealing approach for meeting rising energy needs.[14] CO_2 reduction reactions may be conducted in this technique by electrons/holes following photo-excitation of semiconductor photocatalysts by sun irradiation, which has major benefits since photocatalytic processes can be performed under moderate circumstances.[15,16] The unique feature of photocatalytic CO_2 reduction reactions is the wide variety of CO_2 reduction products, including HCOOH,[17–20] CO,[21–23] CH_4,[24–28] CH_3OH,[29–32] *etc.*, which is mostly determined by the kind of active sites on the photocatalyst's surface.

[a]*College of Materials Science and Engineering Northeast Forestry University, Harbin 150040, China. E-mail: haiyueyang@nefu.edu.cn; wangcy@nefu.edu.cn*
[b]*Key Laboratory of Bio-based Material Science and Technology, Ministry of Education Northeast Forestry University, Harbin 150040, China*

Therefore, along with efforts to produce superior photocatalysts, the exact building of reaction sites that enable adequate selectivity for the desired products has been widely researched for effective photocatalytic CO_2 reduction processes.[33] Because the function of a conventional photocatalytic system is heavily dependent on the energy band structure and surface structure of the catalyst, sluggish separation of electron–hole pairs and a restricted number of surface active sites are still far from satisfactory.[34] The lack of activity and poor output selection severely limit its practical application. In order to enhance the production of the required components as well as better understand the CO_2 reduction reaction process, output selectivity must be tuned.[35] Despite significant efforts, heterogeneous photocatalysts have so far suffered from many shortcomings, such as the inadequate photon absorption efficiency, fast charge carrier complexation, ineffective molecular activation[36] and delayed charge transfer of carriers, which significantly inhibits the transfer of charges from the catalyst surface to reactant molecules and limits the performance of various systems.[37] Therefore, single-atom catalysts have gained attention as prospective photocatalyst candidates due to their distinctive characteristics of very with excellent atomic efficiency and exceptional catalytic performance.[11] In addition to boosting the amount of active sites, for photocatalytic reactions, the separated reaction centres in the single-atom photocatalytic systems are possible to broaden the scope of light collecting as well as enhance the effectiveness of charge segregation and transference. Moreover, with enough light traps and precise surface modification, the created single-atom photocatalyst is highly deployable and can adsorb and activate molecules.[3] In addition, we can draw more precise connections between structure and performance thanks to the structural simplicity of single-atom photocatalysts, which improves our knowledge of the underlying principles of photocatalysis.

It is vital to outline the most recent research developments in single-atom photocatalytic CO_2 reduction so as to encourage the quick growth of this new subject. This may both expose the principle operating mechanism and provide inspiration for future research directions. Although some excellent reviews have summarized the impact of single-atom reaction sites in photocatalysis[3,11,38] in detail and emphasized the approaches to single-atom catalysts manufacturing,[37,39,40] the underlying concept of single-atom photocatalytic reactions and the application of novel CO_2 reduction photocatalysts were not discussed in the reviewed literature, which is crucial to comprehend single-atom photocatalytic CO_2 reduction as well as its prospective large-scale use. In the overview paper, the key principles of single-atom photocatalytic CO_2 reduction are firstly highlighted, so as to fully understand its mechanism of operation and therefore facilitate more efficient framework and preparation of single-atom photocatalysts. Secondly, the production techniques, advantages and disadvantages of single-atom photocatalysts are discussed. Then, the improvement and achievements of three popular photocatalysts for CO_2 reduction processes with TiO_2, g-C_3N_4 and MOFs (metal–organic frameworks) materials as carriers are presented based on the interactions between single atoms and carriers. Finally, we discuss some problems and potential opportunities for single-atom catalyst development in photocatalytic energy conversion.

Achievements and characteristics

In this paper, through the screening and statistics of single-atom photocatalytic CO_2 publications gathered in the CNKI, SCIE, and Springer databases, we find that the number of published papers and related citations and downloads increased exponentially from 2015 to 2022, as shown in Fig. 1 and 2, and this topic was still in a highly discussed stage at the beginning of 2023. In the last decade, the research on single-atom photocatalytic CO_2 shows the characteristics of the rapid growth of talents, extensive application fields, and continuous emergence of results. As one of the typical photocatalytic oxidation–reduction reactions, extensive research on photocatalytic reactions (*e.g.* water splitting) has established a technological basis towards photocatalytic CO_2 reduction reactions.[41] In 2014, Yang *et al.* were the first to disclose the production of hydrogen *via* water using a single-atom catalyst ($0.2Pt/TiO_2$) by photocatalysis, which outperformed metal nanoparticles.[42] Two years later, Zhang *et al.* exhibited that single Co atoms anchored in the metal–organic framework (MOF) significantly promoted the segregation of photoinduced carriers in the MOF-525-Co photocatalyst and augmented the directional mobility of photoinduced electrons from the carriers to the metal center.[43] In 2017, Wei *et al.* further found that the intermediate energy gap state generated in the isolated Co_1–P_4 site anchored g-C_3N_4 photocatalyst may boost light trapping capacity and offer segregation centres to inhibit charge complexation at the same time prolong carrier life.[44] In 2019, Wang *et al.* simulated the structure of chlorophyll and prepared a series of hollow Zr-porphyrin-MOF(HNTM-Au/Cu/CO-SA) photocoupled electrocatalysts supported by Au, Cu and Co atoms. When combined with light, HNTM-Au-SA and HNTM-Co-SA demonstrated excellent CO Faraday efficiencies of 95.2% and 92.2%, respectively.[45] These ground-breaking efforts have significantly aided and sparked the explosive growth of single-atom photocatalytic CO_2.

Photocatalysis is a chemical reaction where catalysts absorb photons to generate energizing electrons and holes, that are

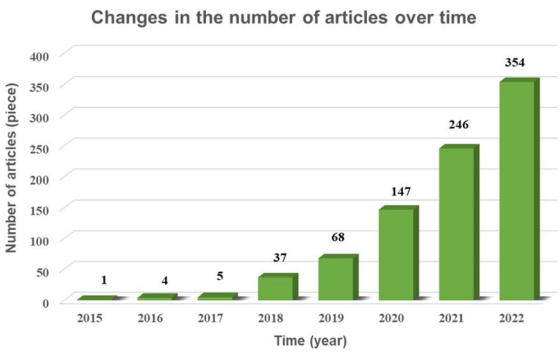

Fig. 1 Graph of number of articles over time.

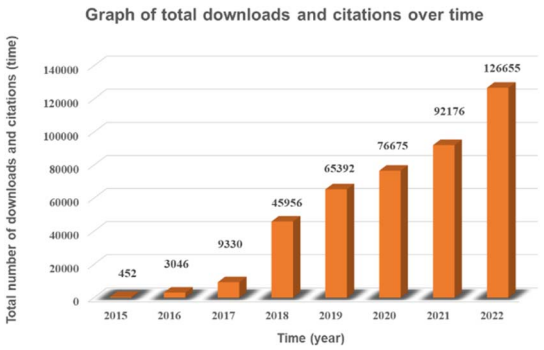

Fig. 2 Graph of total downloads and citations over time.

then used to initiate reduction and oxidation events, respectively.[3,46–48] The photocatalytic water splitting process and single-atom photocatalytic CO_2 reduction process have a similar reaction mechanism. Six stages are involved in the photocatalytic CO_2 reduction process: light absorption, photoexcitation, segregation and transference of photo-generated electron–hole pairs, CO_2 adsorption, interfacial CO_2 reduction reaction, and product desorption.[49]

As depicted in Fig. 3, photocatalysts generate photo-generated electron–hole pairs underneath the influence of incident light, and the excitation wavelength of the incident light is controlled by the energy band structure of semiconductors. Once that energy produced by the incident light exceeds the semiconductor band gap, the excited semiconductor's electrons move from the valence to the conduction band, producing photo-generated electron–hole pairs.[50] The conduction band and valence band of photocatalysts act as reduction/oxidation centres, which will supply electrons to reduce CO_2 and oxidize the water vapor in the reactant mixture, respectively.[51] Therefore, the modification of semiconductor photocatalysts is particularly important for photocatalytic reactions. Doping or solid solution structure can be used to enhance the density of electrons and holes in a photocatalyst, resulting in a broad spectrum of light response and an excellent light absorptivity.[52] The thermodynamic properties of CO_2 molecules are stable, which makes the photocatalytic CO_2 reduction process more complicated. It is challenging to attain an acceptable selectivity since most photocatalytic CO_2 reduction processes have near reduction potentials and there are competitive hydrogen desorption reactions.[53] Furthermore, the bond energy of C=O is 799 kJ mol^{-1},[54] making the activation of CO_2 extremely difficult. The selectivity of products is intimately connected to the diffusion of reactants and intermediaries. Adsorbing CO_2 molecules, decreasing the overpotential of CO_2 reduction, capturing photo-generated electrons to facilitate charge separation, and enhancing selectivity by modifying the desorption energy of intermediaries are all functions of the active centre in a photocatalytic CO_2 process.[55] Furthermore, the efficiency of the photocatalytic CO_2 reduction process is greatly reliant upon that quantity and complete exploitation of reaction sites.[15] Therefore, it is essential to study the mechanism of reaction sites and control the types of reaction sites to trigger photocatalytic CO_2 reduction reactions with good target product selectivity.

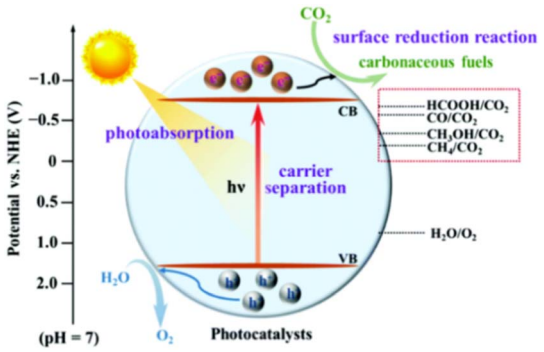

Fig. 3 CO_2 photocatalytic reduction process.[56] Reproduced with permission. Copyright 2020, Royal Society of Chemistry.

Preparation of single-atom catalysts

Because of its substantial advantages in terms of improved light trapping, accelerated charge transport kinetics, and interfacial reactions in photocatalytic systems,[57] single-atom catalysts were proven to be extremely effective in many typical photocatalytic processes, particularly CO_2 reduction. Scientists have made tremendous progress in the investigation of catalysts in synthetic chemistry in recent years, which has tremendously aided in the growth of single-atom catalysts.[58] Due to the high interfacial energy of individual atoms in single-atom catalysts, active sites are easily relocated and aggregated into the clusters and nanoparticles.[59] The coexistence of metal nanoparticles and metal monatomic sites in supported catalysts has been widely accepted by scientists,[60] which provides extra challenges in high-loading active sites. In order to achieve sufficient distance and good distribution between each substance of the metal precursor, prevent metal site agglomeration after reprocessing, and provide enough anchoring positions for stabilizing a single atom, scientists have carried out a variety of synthetic studies.[11] As depicted in Fig. 4A, especially for photocatalytic CO_2 reduction processes, photocatalysts with single-atom reaction sites provide considerable advantages over traditional metal or metal oxide co-catalysts in the type of nanoparticles or clusters because of their distinctive structure.[15] In this paper, we summarized some particular methods for making single-atom catalysts, mainly wet synthesis, atomic layer deposition, co-precipitation method, high-temperature calcination, chemical etching, freeze-drying, microwave-assisted and ball milling, and focused on wet synthesis method, atomic layer deposition method, co-precipitation method and dipping method.

Wet synthesis method

Since it has the advantage of being simple to operate and requiring no additional equipment, wet synthesis is frequently utilized to produce stable single-atom sites.[61] At the same time, wet synthesis offers good dispersibility and deployment.[62] In

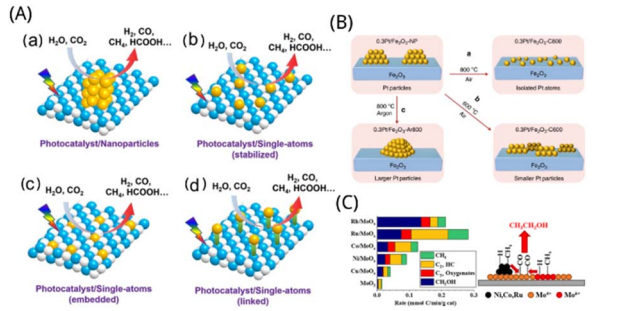

Fig. 4 (A) Water splitting and CO_2 reduction reactions on a photocatalyst containing (a) reactive sites for nanoparticles, (b)–(d) reactive sites for single atoms.[15] Reproduced with permission. Copyright 2021, Wiley-VCH GmbH. (B) Restructuring of Pt nanoparticles caused by heat. (a and b) Calcination in an oxygen or inert environment (c), producing dispersion as single atoms or particle sintering, respectively.[69] Reproduced with permission. Copyright 2019, Nature Communications. (C) Product formation rate and reaction mechanism of Mo-containing catalysts.[77] Reproduced with permission. Copyright 2019, American Chemical Society.

a conventional wet synthesis procedure, metal antecedents in solution (including metal compounds and mononuclear metal complexes) are often supplied to semiconductor substrates by electrostatic adsorption or organic complexation, and then reduced or activated to obtain isolated single-atom reaction sites on the semiconductor.[63]

Biasi *et al.* modified the catalysts with a catalyst wet pretreatment method, which was used for catalysts prepared after modification with different concentrations of aqueous NaBr solutions, and found that bromides have an active role in the reconstitution of the metal phase. They performed wet pretreatment of catalysts with 1% Pd/C catalyst sample (1PdC) using aqueous sodium bromide solution. Two dilute solutions (1.22 and 12.5 mM) were first prepared. Typically, 1.0 g of the original catalyst 1PdC was suspended in 15 cm^3 of water. The modifier was then introduced, an exact aliquot of one of the two starting aqueous solutions (1.22 or 12.5 mM) was added, and the mixture was stirred for 2 h. The final volume of the pretreatment was always adjusted to 30 cm^3. The solids were recovered by vacuum filtration and carefully washed with water (5×5 cm^3) on a Buchner filter. The pretreated mother liquor was concentrated and analysed by ion chromatography to estimate the amount of bromides. Thus, the solid was dried overnight in an oven at 383 K. Approximately 50 mg of all catalysts obtained by the above method were mineralized and analysed for palladium content by ICP-OES.[64] Chen *et al.* used vacancy defects on the layered nitride $Ti_{3-x}C_2T_y$ to load Pt single atoms (Pt loading (mass fraction) was only 0.2%), which showed near 100% conversion and selectivity in the catalytic CO_2 amination reaction at 140 °C. They dispersed 8 mL of $Ti_{3-x}C_2T_y$ MXene suspension in 20 mL of distilled water under magnetic stirring to form clear solution A. Solution B was prepared by adding 10 μL of $H_2PtCl_6 \cdot 6H_2O$ (0.1 g mL^{-1}) solution to 50 mL of distilled water. Solutions A and B were then were sonicated for 1 h and 10 min. Solution B was slowly added dropwise to solution A under stirring. After the reaction for 8 h, $Pt_1/Ti_{3-x}C_2T_y$ was precipitated with acetone for half an hour and collected by centrifugation with acetone to obtain $Pt_1/Ti_{3-x}C_2T_y$.[65] Xu *et al.* compounded a single cobalt atom catalyst (Co–N–C) by an improved template etching method and applied it to the degradation of pollutants. The experimental test found that Co–N–C has more catalytic oxidation activity than Co_3O_4, and the peroxymonosulfate (PMS)/Co–N–C oxidation process with mixed reaction pathway has a broad prospect in removing complex water pollutants. First, they added 0.6 mmol of $Co(CH_3COO)_2 \cdot 4H_2O$ and 1.8 mmol of $C_{12}H_8N_2 \cdot H_2O$ to 60 mL of ethanol and sonicated for 10 min. Second, 3 g of MgO was further added and sonicated for another 15 min. The mixture was then sealed and magnetically stirred at 60 °C (water bath) overnight. After complete evaporation of ethanol, the dried solid was ground into a powder and heated in a tube oven. The oven was fluxed with N_2 at room temperature for 30 min, after which it was ramped up to 700 °C at a rate of 2 °C min^{-1} and maintained for 2 h. The product was stirred in 1 M H_2SO_4 for 4 h to leach out the template MgO and any possible metals or oxides. The acid leaching was repeated 3 times. After washing 5 times with ultrapure water, the solid was dried at 60 °C overnight.[66]

Co-precipitation method

Co-precipitation is a method of adding a precipitant to a mixed metal salt solution so that two or more cations contained in the solution are precipitated together to produce a precipitation mixture or solid solution precursors, which are filtered, washed, and thermally decomposed to obtain a composite oxide.[67] Currently, the main carriers that can be used for the preparation of single-atom catalysts are oxides and carbon nanotubes.[68]

Lang *et al.* prepared 1.8 wt% Pt/FeO_x catalysts, denoted as Pt_1/FeO_x, by co-precipitation method of an aqueous mixture of chloroplatinic acid ($H_2PtCl_6 \cdot 6H_2O$, 37 mg_{Pt} mL^{-1}, 2.6 mL, 99.9%, Sigma-Aldrich) and $Fe(NO_3)_3 \cdot 9H_2O$ (1 mol L^{-1}, 40 mL) with Na_2CO_3 solution (11 g Na_2CO_3 in 100 mL H_2O) at 50 °C under stirring for 3 h, and ageing static for a further 2 h. The obtained solid was recovered by filtration, washed with deionized water and dried at 60 °C overnight. Then a part of Pt_1/FeO_x was calcined at 800 °C according to the above method, and expressed as Pt_1/FeO_x-C800, as depicted in Fig. 4B. The specific activity is significantly higher than that of traditional nanoparticle catalysts because of the resultant large concentration of single atoms. This non-defective stabilizing method may be expanded to non-reducible carriers by easily blended with iron oxide, laying the foundation for development of highly loaded single-atom catalysts for various industrially important catalytic reactions.[69] Extensive studies revealed that the single atoms served as the most important active sites. Lin *et al.* synthesized a series of Ir/FeO_x catalysts with different Ir loadings through a co-precipitation method and HAADF-STEM revealed that the individual Ir atoms occupied exactly the positions of the Fe atoms.[70] To solve the problem of low loading of single-atom catalysts, Ding *et al.* used MnO_2 with special pore structure as a carrier to increase

the loading of noble metals. They prepared Ag/Hollandite-type MnO_2 single-atom catalysts using $MnSO_4$ and $KMnO_4$ as raw materials and $AgNO_3$ as catalyst precursor by co-precipitation method. Hollandite-type MnO_2 was first prepared by hydrothermal method, and then the prepared $[Ag(NH_3)_2]OH$ solution and H_2O_2 solution was added to the MnO_2 suspension.[71] After drying, a loading of about 28.8 wt% of Ag/Hollandite type MnO_2 single-atom catalyst.

Atomic layer deposition method

Because standard techniques of creating catalysts make it difficult to regulate the development and locations of metal particles,[72] atomic layer deposition can control the metal particles as nanoparticles, clusters and single atoms by regulating the number of cycles or deposition sites.[73] A technique called atomic layer deposition (ALD) may deposit materials as single atomic films on the surface of the substrate layer by layer.[74]

Ye *et al.* fabricated the single atom of Pt_1 loaded up to 4wt% on cerium oxide nanorods by atomic layer deposition technology. Ceria defect sites, metal loadings, and high-temperature calcination were discovered to be efficient techniques of tuning the stability of Pt_1 single atoms in the hydrogen atmosphere. It revealed that at the defect and step-edge sites, a single atom of Pt_1 on cerium oxide was largely in the +2 valence state, but the single atom at the step site was in the +4 valence state.[75] Gorey *et al.* prepared Pt–Sn bimetallic catalyst by ALD technology combined with temperature programmed method, in which clusters of Pt_4, Pt_7 and Pt_{24} of sizes ranging were deposited on SiO_2, then hydrogenated, and the seeds of Sn were selectively added by self-limiting reaction with $SnCl_4$. Sn deposition was found to be self-limiting at fairly modest $SnCl_4$ exposures, revealing that the reaction was self-contained, and non-selective Sn deposition efficiency on SiO_2 carriers was 40-fold lower than that on hydrogenated Pt cluster sites. The activity test showed that the catalyst with an alloy structure can obtain higher catalytic performance. They used Pt_4, Pt_7, and Pt_{24} clusters. Mass-selected Pt_n^+ were introduced into the UHV system, where they were deposited on the SiO_2 substrate by means of a 2 mm diameter exposure mask at a distance of 1 mm from the surface. The deposition energy of the Pt clusters was calibrated by delayed potential analysis of the beam on the sample and set to ~1 eV per atom. Deposition was monitored by integrating the neutralization currents, and here all samples contained 1.5×10^{14} Pt atoms per cm^2 (~10% of a dense row of Pt monolayers) deposited as Pt_4, Pt_7, or Pt_{24}.[76] Zhang *et al.* investigated syngas reforming catalysts made from transition metal elements (Ni, Co, Cu, and Ru) loaded on molybdenum oxide which was produced by deposition of atomic layers on silica. Transition metals were added to molybdenum oxide, which significantly improved the catalytic performance. Furthermore, the formation of the CH_x group may be accelerated further by ALD placing a sufficient quantity of transition metal on the Mo active site, thereby facilitating the formation of C_{2+} oxide species, as depicted in Fig. 4C. Bis(*tert*-butylimino)bis(dimethylamino) molybdenum (Strem Chemicals), bis(ethylcyclopentendien) manganese, titanium tetrachloride, and trimethyl aluminum were used as precursors for MoO_x, MnO_x, TiO_x, and AlO_x depositions. Water was used as a coreactant. ALD was done at 623 K with an alternative deposition of MoO_x and TiO_x (AlO_x) with five cycles of deposition of each element for $MoTiO_x/SiO_2$ and $MoAlO_x/SiO_2$. For the $MoMnO_x/SiO_2$, five cycles of MoO_x was deposited at 623 K, after which the reactor was cooled to 523 K to deposit five cycles of MnO_x by ALD.[77]

Dipping method

The dipping method as one of the common methods for the preparation of single-atom catalysts is one of the most common methods for the preparation of single-atom catalysts. The method is to immerse the carrier into the catalyst precursor solution, load the metal ions on the carrier surface by electrostatic adsorption on the carrier surface, and prepare the single-atom catalyst with good catalytic performance by rotary evaporation, drying and reduction processes.[78] Currently, metal oxides,[79] 1D nanowires[80] and 2D nanosheets[81] are often used as carriers for the preparation of single-atom catalysts by the impregnation method.

Kim *et al.* prepared Pt_1/ATO single-atom catalysts using $H_2PtCl_6 \cdot 6H_2O$ as the catalyst precursor and antimony-doped oxidized (ATO) powder as the carrier by the dipping method. They first mixed Pt (1 wt%, 4 w% and 8 wt%) precursor solutions with ATO at different contents, dried and then prepared Pt_1/ATO single-atom catalysts by reduction at 100 °C and 400 °C under H_2 atmosphere, respectively. HAADF-STEM images confirm the presence of Pt single atoms and that Pt single atoms are located on the surface of Sn Sb or SnO_2. Density flooding theory (DFT) calculations show that: the Sb sites in Sn Sb reach their most thermodynamically stable state when they are replaced by Pt. The catalyst showed high catalytic activity, selectivity and durability, and after 1800 cycles, Pt/ATO still maintained high activity in catalytic formic acid oxidation reaction.[82] Zeng *et al.* prepared Pt_1@Fe–N–C single-atom catalysts by impregnation with 2-methylimidazole ($C_4H_6N_2$), ZnO and iron acetate, using H_2PtCl_6 as the catalyst precursor. The Pt_1@Fe–N–C single-atom catalysts with a negative loading of about 2.1 wt% were prepared by adding H_2PtCl_6 solution to the Fe–N–C solution at 70 °C to fully adsorb Pt^{4+}, and then stirred, filtered and dried in Ar atmosphere. After extensive testing, the catalyst showed good durability.[83] Yang *et al.* prepared CoN_4/nitrogen-doped graphene (NG) single-atom catalysts by impregnation method using g-C_3N_4 as the raw material, polyoxyethylene-polyoxypropylene-polyoxyethylene (F127 complex) as the surface active agent and $Co(NO_3)_2 \cdot 6H_2O$ as the catalyst precursor. They first ultrasonically dispersed the g-C_3N_4, $Co(NO_3)_2$ and F127 complex precursors to make the F127-protected Co ions penetrate into the layer of g-C_3N_4, then pyrolyzed the precursors under N_2 atmosphere and finally etched with hydrochloric acid at room temperature to obtain CoN_4/NG catalysts with a loading of about 9 wt% and they exhibited excellent electrocatalytic activity.[81] We list a variety

Table 1 A overview of the supports and fabrication methods used to create supporting single-atom catalysts (SACs) for diverse catalytic processes

Single-atoms	Support	Methods	Applications	Ref.
Pt_1	Co_3O_4	Atomic layer deposition method	Ammonia borane dehydrogenation for room-temperature hydrogen production	84
Pt_1	Ceria nanorods	Atomic layer deposition method	Hydrogen reducing	75
Pt_nSn_x	SiO_2	Atomic layer deposition method	Ethylene binding and dehydrogenation	76
Ni, Co, Cu, Ru	MoO_x/SiO_2	Atomic layer deposition method	Synthesis gas conversion	77
Pt	MOF-NC	Atomic layer deposition method	Oxygen reduction reactions	85
Rh	Phosphotungstic acid	Co-precipitation method	CO oxidation reactions	86
Pt	CeO_2	Co-precipitation method	At 200 °C, the full conversion for the CO shift reaction	87
Pt_1	Co_3O_4	Co-precipitation method	The total oxidation of methanol	88
Pt	g-C_3N_4	Dipping method	Photocatalytic H_2 evolution	89
Pd_1Ag_3	Al_2O_3	Dipping method	Liquid-phase hydrogenation of diphenylacetylene (DPA)	90
Pt–Co	HZSM-5	Dipping method	Dichloromethane catalytic oxidation (DCM)	91
Rh	ZnO	Dipping method	Hydroformylation of olefins	92
CoN	Graphene	Dipping method	Cathode catalyst of Zn air battery	81
Ni	Graphene	Dipping method	Electrocatalytic hydrogen evolution	93
Ni	Graphene	Dipping method	Electroreduction of CO_2	94
Co, Ni, Zn, Pd, Pt	Metal oxides, nitrogen-doped carbon, polymeric carbon nitride	Dipping method and two-step annealing	Sustainable chemical and energy transformations	95
Pt_1	Co nanocrystals	Ball-milling method	5-Hydroxymethylfurfural (HMF) hydrodeoxygenation to 2,5-dimethylfuran (DMF)	96
Pt_1	ZnO	Ball-milling method	Semi-hydrogenation and carbon monoxide oxidation	97
Pt	Ceramic MOF (Ce-MOF)	Low-temperature photoreduction method	CO oxidation	98
Ag	Antimony-doped tin oxide (ATO)	High-temperature cracking method	CO oxidation	99
Ni	Ultrathin 2D graphitized carbon nanosheets	High-temperature cracking method	The conversion of CO_2 to CO	100
Ni	TiO_2 nanoparticles	Molten salt method	Photocatalytic H_2 evolution	101
Fe	Nitrogen-doped porous carbon	Method for thermal emission and trapping with the aid of molten salt	Column 4 cathode oxygen reduction reactions	102
NiCu	SiO_2	Successive reduction method	Ethanol dehydrogenation	103

of loaded single-atom catalysts with single atoms, carriers, fabrication methods and their applications, as shown in Table 1.

Advantages of single-atom catalysts in photocatalysis

It is crucial to investigate advantageous heterogeneous catalysts if alternative sources of energy like biomass, solar, or nuclear are to be used in the future.[104,105] Single-atom catalysts offer enormous possible application in metal resource rationalization and the creation of an atomic economy.[106] Moreover, loaded single-atoms have demonstrated significant promise in heterogeneous catalysis because of their improved activity, stability, and selectivity, as well as their peculiar electronic structure and unsaturated coordination centres.[107] Single-atom catalysts that integrate separated single metal atoms on suitable supports, therefore open up new possibilities for heterogeneous catalysts in terms of the material fabrication and possible applications for various catalytic processes.[108] We briefly outline the

substantial benefits of single-atom catalysts for photocatalytic reactions in the following four categories in this paper.

Improved metal utilization

Nanostructured materials have been extensively researched as heterogeneous catalysts for various catalytic processes.[109] Despite the significant accomplishments of traditional nanocatalysts, they still continue to be numerous obstacles to overcome.[110,111] Hardly no metal atoms accessible to the reaction mixture may function as catalytically active sites upon a cost standpoint, which results in the unsatisfactory usage efficiency of metal atoms (particularly for nobel metals).[108] A single-atom catalyst is a revolutionary form of catalyst that has reactive metal atoms scattered on the substrate separately.[112] High dispersion of single atoms with good stability allows each atom to be exposed as a catalytically active site.[113] Constructing single-atom reaction sites is beneficial to maximize the usage of metal active centres for catalytic processes.[114] The homogenous and well-dispersed active centres give an approximately 100% usage of metal atoms,[115] increase the usage of precious metals, and accomplish the cost-effectiveness goal, which is also one of the initial goals of preparing single-atom catalysts.[116]

Carbon-based ones offer outstanding qualities like as cheap cost, various structures, excellent stability, and strong conductance, and are thus commonly employed as SACs carriers.[117] In the carbon skeleton, there exists a tight contact between metal atoms and neighboring carbon atoms, which changes the carrier concentration and electronic structure of metal atoms and promotes the development of new active sites within nearby carbon atoms.[118] As a result, the carbon-based equipped metal monoatomic catalyst's atom usage rate is nearly 100%,[119] resulting in high energy conversion efficiency while lowering expenses. Economic gains and energy sustainability can be realized *via* constructing a distinctive structure of the catalyst.[120] Wang *et al.* demonstrated an effective strategy for the simultaneous design of Pd SAs, clusters and V_Os on TiO_2, resulting in enhanced photocatalytic activity for H_2 production and selective oxidation of benzylamine at a very low Pd loading cost with greatly improved atom utilization. The optimized Pd_{SA+C}/TiO_2-V_O photocatalysts showed higher yields of H_2 and *N*-benzylidene benzylamine than the Pd_{SA}/TiO_2-V_O containing only Pd SAs and other related photocatalysts.[121] Chen *et al.* investigated Pt/TiO_2 (anatase) sac for the reverse water–gas shift (rWGS) reaction. The potential of Pt single atoms (Pt_1) for catalytic conversion is initially masked by their saturated coordination with TiO_2 and can be released by reduction-oxidation treatment. We show that a controlled reducing atmosphere moves Pt_1 to form small amorphous aggregates that can be redispersed into Pt_1 by mild oxidation. Redispersed Pt_1 shows less coordination to surface O than Pt_1 of fresh catalysts, hence better accessibility and consequently higher activity in the rWGS reaction.[122]

Enhanced reaction activity

From the viewpoint of photocatalysis, light harvesting, charge creation and segregation, and catalytic reaction are the three fundamental reaction stages in a photocatalytic process. The total efficiency of a photocatalytic system is governed in this way by the equilibrium of kinetics and thermodynamics of these three major reaction stages.[3] However, photocatalysis is hampered by fast coupling of photoexcited charge carriers and a scarcity of active sites for catalytic processes, culminating in disappointing results that disconnected from practical use. Along with their special geometric and electrical properties, single metal atom catalysts not only boost the amount of active sites owing to maximal atom-utilization efficiency, and moreover improve the fundamental activity of the each active site.[123] What is more, for photocatalytic reactions with single atom reaction sites, semiconductors are the carriers of metal active centres and primary catalysts to provide photo-generated charge carriers to promote photocatalytic reactions,[124] and single atoms attached to the surface of the photocatalyst serve as the reaction sites for oxidation and reduction. Charge separation is facilitated by photocatalysts with single atomic reaction sites,[44] and it is helpful to change the electronic band structure of photocatalysts,[125] thus Increasing activity through boosting light reception and photocarrier transmission. Furthermore, the unsaturated single atom contributes to the adsorption, activation together with selective conversion of CO_2 molecules. Moreover, the surface structure of single-atom photocatalysts can enhance photocatalyst adsorption, activity and chemical stability through different metal-carrier interactions. Zeng *et al.* pretreated graphite carbon nitride (GCN) with H_2O_2 to introduce active C–OH groups capable of reacting with $HAuCl_4$ to fix monatomic Au(I) in the GCN matrix *via* solid Au(I)–O coordination bonds. In the photocatalytic hydrogen evolution process, this mutual interaction can effectively limit the migration of intermediate Au(0) towards the production of Au particles. As a result, the single atom Au(I) integrated GCN demonstrated higher activity and stability for photocatalytic hydrogen production.[126] Wang *et al.* prepared porous titanium dioxide loaded copper single-atom ($Cu–SAs/TiO_2$) photocatalysts and found that the total yield of CH_4 and CO from CO_2 photoreduction on $Cu–SAs/TiO_2$ reached 34.64 μmol g_{cat} h^{-1} with good activity and stability of the photocatalyst when a small amount of oxygen (117.6 ppm) was added to the reaction system. This is because the competing electron transfer to O_2 on $Cu–SAs/TiO_2$ maintains the dynamic stability of the $Cu^{\delta+}$ active centre, the O_2-derived *OOH species reduces the formation energy barrier of the key intermediate *COOH, and the transfer of *H species accelerates the intermediate protonation process.[127]

Improved photocatalytic stability and selectivity

The interfacial free energy of metals grows significantly with decreasing particle size, from nanoparticles and sub-nanoclusters to individual metal atoms. Metals' interfacial free energy rises dramatically as particle size decreases. As a result, the mutual interaction between active sites and metal atoms becomes stronger.[118] Thus individual metal atoms have stronger metal–atom–carrier interactions and are more stable. As a single atom is chemically anchored on the supporting

photocatalyst, a single metal atom is firmly bonded with the adjacent anchoring sites, which raises the specific surface area, modifies the bonding and coordination environment of atoms, and forms a unique low coordination active centre structure with strong site activity and high uniformity.[128] Therefore, single-atom catalysts demonstrate greater specific catalytic activity, stability, selectivity, as well as catalytic efficiency over typical nanoparticle-based multiphase catalysts For some photocatalytic processes.[129] Nie *et al.* discovered a novel sort of active site on CeO_2 near the ionic platinum Pt^{2+} that exhibited increased activity. Such active sites may be stabilized in an oxidative atmosphere when the temperature reaches 800 °C.[130]

Single atoms have an evenly distributed, firmly attached, and often electron-deficient character. By varying the manner and intensity of the reaction mixture, intermediate, and/or output adsorption, or by altering the reaction route, one may control the selectivity of the reaction.[104] By using a straightforward deposition technique, Huang *et al.* created photocatalysts with single Co^{2+} sites on C_3N_4 and showed high activity and product selectivity for CO production. Under visible-light irradiation, a turnover number of over 200 was achieved for the generation of CO employing the synthesized photocatalyst. The existence of single Co^{2+} sites on C_3N_4 and their critical role in accomplishing selective CO_2 reduction were verified by further X-ray absorption spectroscopy experiments.[131] Wang *et al.* demonstrated a voltage-measured electro filtering approach for the ambient temperature production of single-atom catalysts. Following the anchoring of the iron single atom, the free energy of the attracted CO decreases from +0.61*e* to 0.27*e*, so that the electrons can be transferred out of the 3d orbital of iron into the orbital of CO. Fe–SAs/N–C were shown to show outstanding photocatalytic performance for the conversion of aqueous CO_2 to syngas with a controllable CO/H_2 ratio when exposed to visible light. CO and H_2 have gas evolution rates of 4500 and 4950 μmol g^{-1} h^{-1} for CO and H_2, respectively.[132] Additionally, the capacity of the metal atoms to attract other substances may be diminished and selectivity can be increased by alloying the metal atoms in single-atom photocatalysts[133] and altering the electronic structure of the active core atom by the ligand atoms.[134] Wang *et al.* designed and constructed a $Cu^{\delta+}/CeO_2$–TiO_2 photocatalyst through the pyrolytic conversion of Cu^{2+}–Ce^{3+}/MIL-125-NH_2 precursor. In the designed photocatalyst, TiO_2 acts as a light-trapping material for the generation of electron–hole pairs effectively separated by CeO_2–TiO_2 interface, and the Cu–Ce dual active sites synergistically promote the generation and dimerization of *CO intermediates, thus reducing the energy barrier of C–C coupling. The $Cu^{\delta+}/CeO_2$–TiO_2 photocatalyst showed a productivity of 4.51 μmol^{-1} g_{cat}^{-1} h^{-1} and a selectivity of 73.9% for the conversion of CO_2 to C_2H_4 under simulated sunlight with H_2O as the hydrogen source and hole scavenger.[135]

Pointing the way to photocatalysis research at the atomic level

The simple geometry and electronic structure of single-atom photocatalysts,[136] the variety of preparation methods,[137] and the ease of identifying and understanding the reaction mechanism of single atoms as active sites[138] facilitate the atomic-scale research of structure–activity connections and point the way to other photocatalytic studies at the atomic level. Wang *et al.* designed a Z-Scheme photocatalyst with N N–Cu_1–S single-atom electron bridge (denoted as Cu-SAEB) for mediating CO_2RR. In the absence of sacrificial agent, the yields of CO and O_2 on Cu-SAEB were as high as 236.0 and 120.1 μmol g^{-1} h^{-1}, respectively, which exceeded most of the previously reported photocatalysts. The designed Cu-SAEB was highly stable over a total of 30 reaction cycles of 300 h due to the enhanced contact interface of Cu-SAEB and modulated by the atomic structure of N–Cu_1–S. Moreover, N–Cu_1–S acts as SAEB to achieve an effective Z-Scheme charge transfer mode at the contact interface of Cu-SAEB, thus maintaining the photogenerated carriers with strong redox potential and ultimately enhancing the photocatalytic CO_2 performance. This study provides a new direction for the design of highly active photocatalysts with atomic precision and demonstrates the role of interfacial structure in the photocatalytic process.[139]

Disadvantages and improvements of single-atom catalysts

Although single-atom catalysts have many advantages mentioned above, they also have some limitations. When the metal particles are reduced to the single-atom level, the specific surface area increases dramatically, leading to a sharp increase in the free energy of the metal surface,[140] which can easily cause agglomerative coupling to form large clusters during preparation and reaction, thus resulting in catalyst deactivation and affecting the activity and stability of the catalyst.[141] In addition, single-atom catalysts require high structural characterization instruments and complex analysis of catalytic reaction mechanisms, which are engineering technical problems.[142] In some reactions, strong interactions between intermediates and transition metal single atoms may deactivate the reaction sites.[143] During the application of defective engineering to synthesize single-atom catalysts, the conjugation can be weakened, leading to electron–hole complexation, which can also disrupt charge transport and damage the carrier structure,[144] affecting its performance. High stability, high activity and high loading are the great challenges for single-atom catalysts.

The synergistic effect of single metal atoms and carriers can prevent the atomic diffusion of individual metal atoms from aggregating into particles, and the metal oxide carriers can directly participate in the activation of catalytic substrates, making the single-atom catalyst carriers promote the proximity effect of catalytic reactions and substantially enhance the activity of single-atom catalysts.[145] Therefore, choosing a suitable carrier is an effective way to alleviate the above-mentioned defects of monatomic catalysts. Therefore, we found that to improve the performance of single-atom catalysts it is not enough to study just the metal single atoms. The choice of the carrier plays a crucial role in improving single-atom catalysts.[146] It has been shown that the interaction between the metal and the carrier is often used to stabilize the metal particles with the

aim of obtaining highly stable and long-lived catalysts. The carriers in loaded metal catalysts not only play the role of dispersing and stabilizing metal nanoparticles, but also interact with metal particles,[147] which often leads to interfacial charge transfer, metal structure change, molecular adsorption modulation and other phenomena, and in turn affects the activity, selectivity and stability of catalysts.[148]

Commonly used carriers for single-atom catalysts are also abundant, mainly metals and metal oxides, such as Fe_2O_3, TiO_2 and Al_2O_3.[149] In addition, carbon-based carriers are also commonly used as catalyst carriers, such as carbon nanospheres, carbon nanofibers, graphene, metal–organic framework-derived carbon, covalent triazine framework, carbon nitride and phthalocyanine derived carbon, *etc.*[150] TiO_2 is an inexpensive, non-toxic and chemically stable metal oxide with three crystalline phases, rutile, anatase and plagioclase, which are commonly found in nature. Among them, rutile and anatase TiO_2 have been widely used as catalyst carrier materials.[151] Among the many carriers for SACs, carbon-based has excellent properties, such as low price, diverse structure, excellent stability and good electrical conductivity, and is widely used as a carrier material for SACs.[117] Carbon-based carriers are able to introduce heteroatom anchor sites and immobilize metal single atoms; heteroatom-doped carbon can also play a positive role in photocatalytic processes.[152] Carbon materials are preferred as carriers for catalysts, including carbon nanospheres, carbon nanofibers, graphene, metal–organic framework-derived carbon, covalent triazine framework, carbon nitride and phthalocyanine derived carbon.[153] In this paper, we focus on the important roles of three widely used carriers, TiO_2, g-C_3N_4, and MOFs, in improving single-atom catalysts.

TiO_2

Apart from the role of the metal oxide carrier of single-atom catalysts as a ligand to stabilize the catalytic metal center, the metal atoms on the carrier adjacent to the single-atom dispersed metal center may also directly participate in the activation of the reactants and catalytic reaction, forming a significant proximity effect that enhances the catalytic performance, making the real active sites of the atom-dispersed metal catalysts may go far beyond the isolated metal atoms themselves.[154]

In TiO_2-loaded single-atom palladium catalysts, the Pd–O–Ti(III) atomic-level interface formed around the palladium can effectively activate oxygen to form superoxide ions at room temperature, giving the catalysts superior low-temperature catalytic carbon monoxide oxidation activity and excellent performance in the oxidative elimination of greenhouse gases (*e.g.*, methane) and volatile organic pollutants (*e.g.*, toluene).[155]

Liu *et al.* found that the Ti(III)–O–Pd interface in the atomically dispersed Pd_1/TiO_2 catalyst activated O_2 to superoxide, thereby promoting catalytic oxidation, as depicted in Fig. 5A.[155] Due to the unique O_2 activation mechanism, the Pd_1/TiO_2 catalyst reported in this work exhibits the highest CO conversion frequency among the previously reported Pd-based

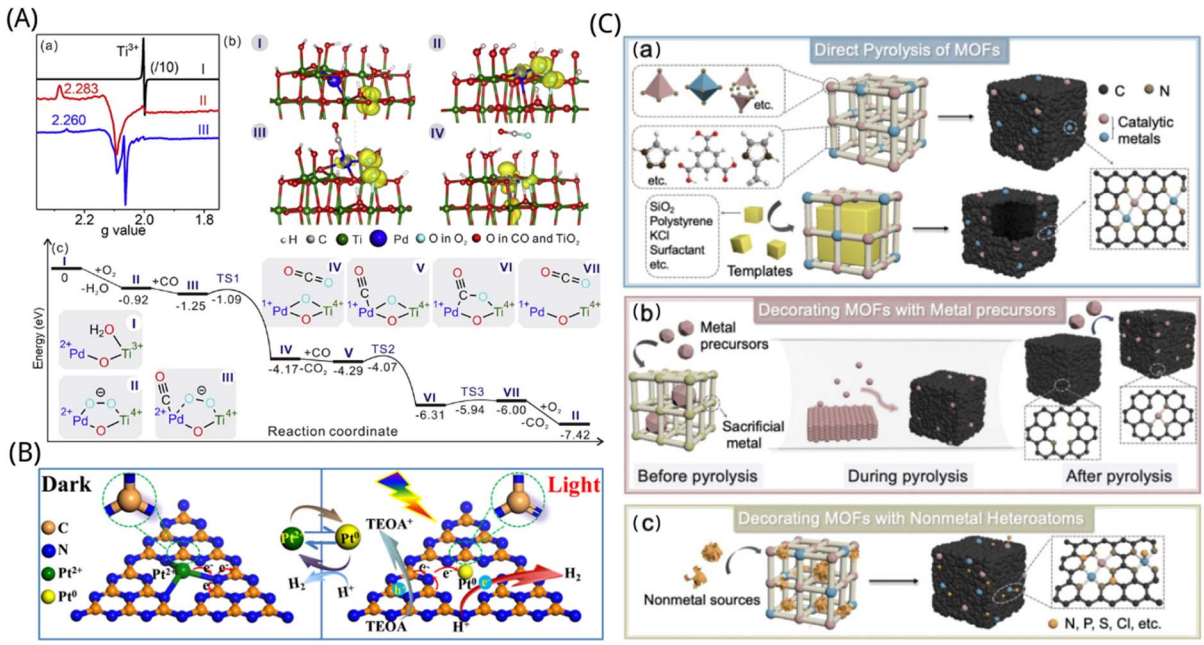

Fig. 5 (A) Mechanism of Ti(III)–O–Pd(II) interface to promote CO oxidation. (a) EPR signal for monitoring the catalytic reaction and (b) structural model showing the spin state of the stable intermediate. (c) Energy of intermediates and transition states in the CO oxidation mechanism at the Ti(III)–O–Pd(II) interface calculated by DFT.[155] Reproduced with permission. Copyright 2018, Elsevier. (B) Illustration of charge transfer and bond variation on S–Pt–C_3N_4 catalysts for photocatalytic hydrogen evolution. TEOA = triethanolamine.[162] Reproduced with permission. Copyright 2020, Wiley-VCH GmbH (C) schematic diagram of the conversion of MOFs to sac by pyrolysis in ORR applications. (a) Direct pyrolysis of MOFs. (b) Decoration of MOFs with metallic precursors. (c) Modification of MOFs with non-metallic heteroatoms.[167] Reproduced with permission. Copyright 2021, Elsevier.

catalysts and enhances the catalytic effect on the combustion of hazardous volatile organic compounds and greenhouse gases. The direct engagement of metal atoms on oxide carriers suggests that the actual active sites of the atomically dispersed metal catalysts may extend well beyond the isolated metal atoms themselves.[156]

g-C_3N_4

Non-precious metal single-atom materials have received much attention in photocatalysis because of their low cost, high reactivity, high selectivity and high atomic utilization.[157] However, the high surface energy of individual atoms causes agglomeration during preparation and catalytic measurements, leading to damage of the catalytic sites.[141] Strong interactions between substrates and single atoms are a key factor in preventing the agglomeration of individual metal atoms and can modulate the geometry and electronic structure of the catalyst to optimize catalytic activity. Nitrogen-doped porous carbon has been widely investigated as an ideal non-precious metal single-atom carrier due to its multi-level pore structure, high specific surface area and defect effect,[158] which synergistically enhances the catalytic performance for oxygen reduction reactions, oxygen precipitation reactions, hydrogen precipitation reactions, and carbon dioxide reduction reactions.[159]

In general, more charge transfer between the low-coordinated non-precious metal single atoms and the strongly electronegative N atoms changes the electron distribution around the metal single atoms, and stronger chemical bonds are formed between the metal single atoms and the carriers, enabling a stronger and more stable dispersion. On the other hand, the defect effect caused by N doping and the intrinsic defects of the carbon material provide additional anchor sites for the metal single atoms.[160] In addition, N doping sites provide confined space for metal single atoms by modulating the porous channels of carbon materials.[161]

It was demonstrated through the experiments of Zhang *et al.* that the Pt^{2+} atom can effectively attract electrons from the C_3N_4 planar layer and convert to Pt^0 atoms under light illumination, accompanied by Pt–N bond breakage, as shown in Fig. 5B. At the same time, the reverse conversion of the –C–N to –C=N bond and the reconstruction of the C_3N_4 molecular structure occurred, which has been confirmed by the similarity of the C 1s and N 1s spectra of S–Pt–C_3N_4 in the excited state to the C 1s and N 1s spectra of primitive g-C_3N_4 in the ground state. Consequently, in the excited state, a single Pt^0 atom with abundant electrons and a C_3N_4 layer with abundant holes in the isolated state can participate in the reduction and oxidation of water, respectively, and the photocatalytic H_2 precipitation performance of single-atom Pt/C_3N_4 is significantly higher than that of Pt-particle-C_3N_4 and C_3N_4.[162]

MOFs

For MOF-immobilized single-atom catalysts based on MOF, the atomic metal sites can be stabilized in the metal nodes, pore spaces or organic ligands of MOF.[163] Compared with other carriers, MOF-immobilized single-atom catalysts have the following advantages. Firstly, three-dimensional ordered porosity is the main feature of MOF-immobilized single-atom catalysts, which can greatly promote the mass transfer process during the reaction and thus improve the catalytic efficiency.[164] Moreover, MOF has rich chemical tunability, which can easily and precisely control the structure of the immobilized single-atom catalytic sites, thus making the prepared atomic-level metal catalysts rich in structural diversity.[165] In addition, embedding atomic-level catalytic active sites in MOFs can achieve a significant increase in the activity of the non-homogeneous catalysts without compromising their long-lasting stability and reproducibility. What's more, by introducing more than one type of metal-based sites at the same time, synergistic interactions between different chemical components in the MOF can be effectively achieved, thus improving the catalytic performance. Last but not least, in general, catalysts prepared using MOFs can usually achieve a high loading of metal content.[166] Hu *et al.* found that the strategy of converting MOFs into sacs by pyrolysis can be divided into three stages. Firstly, MOFs, including pristine MOFs and MOFs with hard/soft templates, are directly converted to sac by high temperature treatment. In the second stage, MOFs are modified with additional metal precursors by various methods. In the final stage, MOFs are combined with components containing nonmetallic heteroatoms to provide more coordination atoms and modulate the electronic structure of the active metal centre, as depicted in Fig. 5C.[167]

Novel single-atom photocatalysts for CO_2 reduction

With to the growth of constant technology and the enhancement of people's environmental awareness, new single-atom photocatalysts for CO_2 reduction are emerging. In this paper, we mainly focus on three popular single-atom photocatalysts of TiO_2, g-C_3N_4 and MOFs materials based on the interaction between single atoms and carriers.

TiO_2

The benefits of the photocatalytic reduction technique are its lack of toxicity, low energy need, and absence of secondary emissions. Widespread interest has emerged in CO_2 photocatalytic reduction processes over TiO_2-based catalysts.[168] In 1979, Inoue *et al.* found that photocatalytic reduction of CO_2 into CH_3OH, HCOOH, CH_4, *etc.* could be done by utilizing TiO_2, CdS, SiC and other photosensitive semiconductor powders suspended in water as catalysts, and explained the kinetics of the photocatalytic reaction based on the charge transfer theory of photoexcited semiconductors,[169] which was the first proposal of the reaction principle of photocatalytic reduction of CO_2. The reaction equation is shown below. After continuous research, it was found that TiO_2 as the most favoured photocatalyst[170] can not only catalyse the conversion of CO_2 into commercially viable organic compounds, but also remove pollutants in the atmosphere such as mercury by photocatalytic oxidation,[171] which

has a good application value and prospect compared with traditional emission reduction technologies.

$$CO_2 + e^- \rightarrow CO_2^-,\ E = -1.9\ eV \quad (1)$$

$$CO_2 + H^+ + 2e^- \rightarrow HCO_2^-,\ E = -0.49\ eV \quad (2)$$

$$CO_2 + 2H^+ + 2e^- \rightarrow CO + H_2O,\ E = -0.53\ eV \quad (3)$$

$$CO_2 + 4H^+ + 4e^- \rightarrow HCHO + H_2O,\ E = -0.48\ eV \quad (4)$$

$$CO_2 + 6H^+ + 6e^- \rightarrow CH_3OH + H_2O,\ E = -0.38\ eV \quad (5)$$

$$CO_2 + 8H^+ + 8e^- \rightarrow CH_4 + 2H_2O,\ E = -0.24\ eV \quad (6)$$

$$2H^+ + 2e^- \rightarrow H_2,\ E = -0.41\ eV \quad (7)$$

$$H_2O \rightarrow \tfrac{1}{2}O_2 + 2H^+ + 2e^-,\ E = 0.82\ eV \quad (8)$$

Due to the TiO_2's high band gap, the photocatalytic reaction's solar light usage efficiency is poor. In order to optimize visible light consumption and TiO_2 activity, it is necessary to dope and modify TiO_2. The methods mainly include non-metal doping, metal cocatalyst deposition, heterostructure construction *via* coupling with other semiconductors, and organic photosensitizer modification. When metal is used to modify TiO_2, charge carriers are moved from semiconductor to metal because of the different Fermi energy levels, enhancing the effectiveness of photo-generated transfer of electrons. Simultaneously, the Schottky energy barrier forms on the surface of the metal–TiO_2, inhibiting the coupling of photo-generated electrons and holes and therefore enhancing TiO_2's photocatalytic efficiency. At present, the metals that are widely used mainly include Pt, Ag, Au, Pd, Ru, Rh, *etc.*

TiO_2 is a suitable supporting material for constructing single-atom photocatalysts based on metal–oxygen bonding configuration. Scientists synthesized single-atom photocatalysts based on TiO_2 materials usually through the sol–gel technique, hydrothermal synthesis, and chemical vapor deposition.[172] Pan *et al.* developed a binary component catalyst made up of single atoms (SAs–Pt and Au) anchored on self-doped TiO_2 nanotubes (TNTs) to promote the effective transition of photo-generated electrons from defect sites to SAs *via* covalent interactions, which improved electron–hole pair separation and charge carrier transfer. The photocatalytic CO_2 reduction efficiency of the Pt–Au/R-TNTs with 0.33 weight percent of SA metals was up to 149-fold more than that of unmodified R-TNT, and the overall apparent quantum yield (AQY) was 17.9%, with yields of CH_4 and C_2H_6 reaching 360.0 and 28.8 μmol g^{-1} h^{-1}, respectively.[173] Compared with other metals, the benefits of the Cu element include affordability and low environmental impact, that may effectively increase photo-generated electron and hole segregation in the catalyst and broaden the spectrum absorption range. Therefore, scientists have undertaken substantial study on the metal Cu–TiO_2 combination. Yu *et al.* suggested that the interaction of metal alloy nanoparticles (NPs) with single atoms might enhance catalytic performance. Therefore, they co-loaded the Cu SAs and Au–Cu alloy NPs on TiO_2 to obtain the excellent performance photocatalyst by photo-deposition, as shown in Fig. 6A. The combinatorial action of Cu SAs and Au–Cu alloy NPs may improve the activation of CO_2 and H_2O adsorption and decrease the overall intrinsic limitations for CH_4 and C_2H_4 production. The yields of 3578.9 mol g^{-1} h^{-1} for CH_4 and 369.8 μmol g^{-1} h^{-1} for C_2H_4 make the production of sunlight-driven high-value solar fuels more feasible.[174] Yin *et al.* further developed Cu single atoms anchored on nitrogen-doped carbon on TiO_2, which showed 100% CO selectivity and high epitaxial quantum efficiency up to 2.0% for photocatalytic CO_2 reduction with H_2O vapor at 420 nm.[175] SAs synthesis and characterization are shown in Fig. 6B. Lee *et al.* demonstrated the atomic-level CO_2 photoreduction reaction on TiO_2 photocatalysts with uniform and stable transition metal single atoms and found that the interaction of electrons with individual Cu atoms and neighboring TiO_2 affects the reduction on the TiO_2 surface, resulting in the automatic establishment of O-vacancies in the vicinity of copper atoms. Therefore, they controlled the space allocation of homogeneous individual copper atoms on TiO_2 as to allow adjacent copper atoms to participate in the mutual effect with CO_2 intermediates through controlled charge positioning. In comparison to the original TiO_2, the improved Cu_1/TiO_2 photocatalyst exhibits a 66 times better CO_2 photoreduction capability.[176] Through the fixing of a single tungsten (W) atomic site with oxygen coordination on the intrinsic step of classical TiO_2 nanoparticles, Feng *et al.* created a unique "single atomic site on an atomic step" approach. The composition of the active site for CO_2 reduction may be adjusted by modifying the extra W^{5+} to produce a W^{5+}–O–Ti^{3+} site, resulting in a CO_2 reduction efficiency of 60.6 μmol g^{-1} h^{-1} and a CH_4 selectivity for CO that exceeds that of pristine TiO_2 by an order of magnitude.[177] The fundamental principle of CO_2 photocatalytic reduction in different reaction systems is a direction well worth discussing. Chen *et al.* used a template-assisted *in situ* pyrolysis approach to synthesize a Cu single-atom-incorporated three-dimensional-ordered macro-porous TiO_2 ($Cu_{0.01}$/3DOM-TiO_2) photocatalyst. The 3DOM TiO_2 framework that the Cu single atoms are evenly embedded in, not just to widens the spectrum of light absorption, and moreover offers particular active sites for the adsorption and conversion of CO_2 molecules. In the gas–solid system, the $Cu_{0.01}$/3DOM-TiO_2 photocatalyst showed excellent selectivity and activity yet it tended to produce C_2H_4 in the liquid–solid system. With a selectivity of 83.3% and a generation rate of 43.15 μmol g^{-1} h^{-1}, the photocatalytic CO_2 reduction process in the gas–solid system primarily produced CH_4, whereas the reaction in the liquid–solid system produced C_2H_4 as the major output with a selectivity of 58.4% and a formation rate of 6.99 μmol g^{-1} h^{-1}.[178] By rationally designing photocatalysts and fine-tuning the reaction conditions, this study contributes a few new knowledge on boosting photocatalytic CO_2 reduction to desired products. Except for the application of such photocatalysts to reduce CO_2 to hydrocarbons, the organic fertilizer urea can also be made catalytically with inorganic substances such as N_2. Li *et al.* used a photoinduction approach based on TiO_2 photocatalyst coupled with reversible monatomic copper (expressed as Cu SA–TiO_2) to produce a moderate

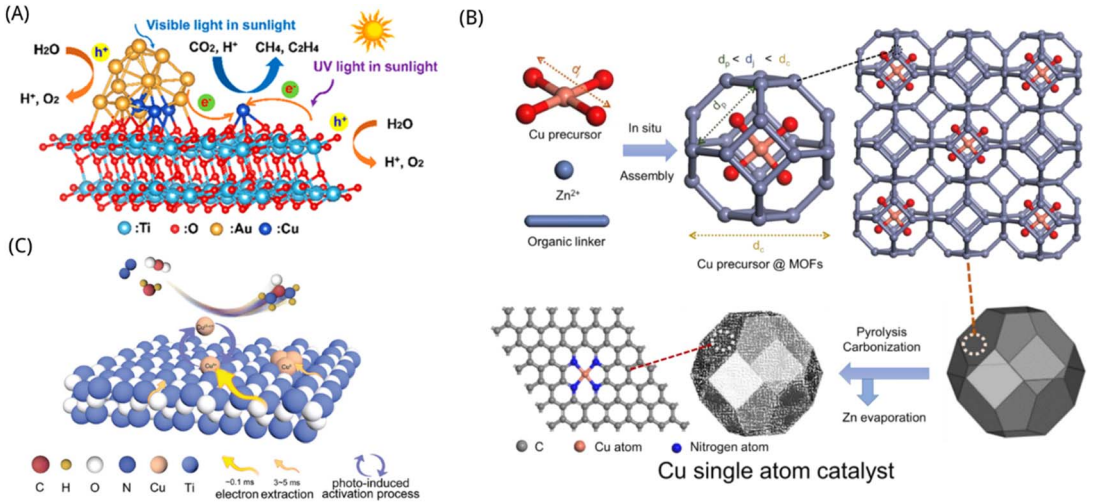

Fig. 6 (A) Diagrammatic representation of the photocatalytic CO_2 reduction process by $Cu_{0.8}Au_{0.2}/TiO_2$.[174] Reproduced with permission. Copyright 2021, American Chemical Society. (B) The scheme for fabricating Cu single atoms site catalysts.[175] Reproduced with permission. Copyright 2022, American Chemical Society. (C) Diagram of urea photosynthesis on the surface with a variety of photocatalysts (pure TiO_2, Cu SA–TiO_2, and Cu^0–TiO_2).[179] Reproduced with permission. Copyright 2022, Wiley-VCH GmbH.

photocatalytic production of urea utilizing N_2 and CO_2 molecules in the environment of pure H_2O, as shown in Fig. 6C. The urea yield was as high as 432.12 μg g_{cat}^{-1} and the speed of photogenerated electron extraction was over 30-fold higher than that of the reference photocatalyst.[179]

Photocatalytic CO_2 reduction by TiO_2-based photocatalysts has a promising future in emission reduction and energy redevelopment. However, owing to the defects of high recombination probability of photo-generated electron–hole pairs, poor CO_2 adsorption performance of catalyst and difficulty in CO_2 activation, and the poor rate of solar energy usage (especially in visible light), its catalytic efficiency is limited.[180] Construction of TiO_2-based single-atom photocatalysts is definitely a good way to realize efficient photocatalytic CO_2 reduction performances. At present, the research has achieved good results and the catalytic efficiency has been significantly improved. Nevertheless, the main research area is dominated by noble single-atom metals and the fabrication method is relatively complicated. Further research is still needed to produce inexpensive, environmentally friendly and universally applicable photocatalysts based on TiO_2 materials.

g-C_3N_4

Graphite nitrogen carbide (g-C_3N_4) has a band gap of 2.7 eV, which is a semiconductor with photocatalytic performance beneath visible light. It has a wider wavelength utilization range of sunlight the TiO_2.[181] Moreover, the catalyst is composed of two common nonmetallic elements, C and N, and has the characteristics of non-toxicity, no pollution, low preparation cost, *etc.*[182] Its physical and chemical properties are stable at normal temperatures and pressure. Therefore, g-C_3N_4 has been extensively studied as a possible nonmetallic semiconductor photocatalyst. However, its high carrier recombination efficiency and low specific surface area reduce the photocatalytic activity of g-C_3N_4. Photocatalysts based on g-C_3N_4 often have poor charge separation and CO_2 adsorption capabilities, which have a negative impact on their capacity to reduce CO_2. Therefore, we can modify the original catalyst in different aspects by preparing composite materials or chemical doping to obtain high photocatalytic performance.

Nano-materials can greatly increase the contact area of catalytic reaction, so most of the g-C_3N_4 on the modified photocatalyst is found as nanotubes. Qin *et al.* synthesized ultrathin nanosheet g-C_3N_4 (NS-g-C_3N_4) by calcination method, as shown in Fig. 7A. Their extremely thin nanostructures and plentiful surface defect sites significantly increase visible light adsorption efficiency along with the segregation and transmission of photo-generated electrons, and provide powerful chemisorption sites for CO_2. Moreover, the surface defects of the nanosheets can contribute to the selective photodegradation from CO_2 to CO, and thus provide significant activity, selectivity and stability for the photocatalytic CO_2 reduction process. They developed NS-g-C_3N_4 with a layer thickness of 10 nm that was more efficient than its bulk equivalent (B-g-C_3N_4) for the photocatalytic reduction of CO2 beneath the illumination of solar light, with CO being the sole product found in the system and yielding 5.8-fold more than B-g-C_3N_4.[183] To modify the g-C_3N_4 photocatalyst's capacity for light absorption, redox potential, and electron removal efficiency, Liu *et al.* fabricated pore-like carbon nitride (g-C_3N_4) nanotubes. Moreover, they also added the appropriate quantities of translucent zeolite imidazolium framework-8 (ZIF-8) nanoclusters to the equipped tubular g-C_3N_4 to improve its capacity for capturing CO_2. Through the collaborative impact of semiconductor nanostructure and surface metal–organic framework grafting agent, the improved ZIF-8 modified tubular g-C_3N_4 photocatalysts shown a remarkable increase in photocatalytic CH_3OH process performance, which is three-fold more than the traditional block g-C_3N_4 (BCN) photocatalyst made *via* melamine pyrolysis.[184]

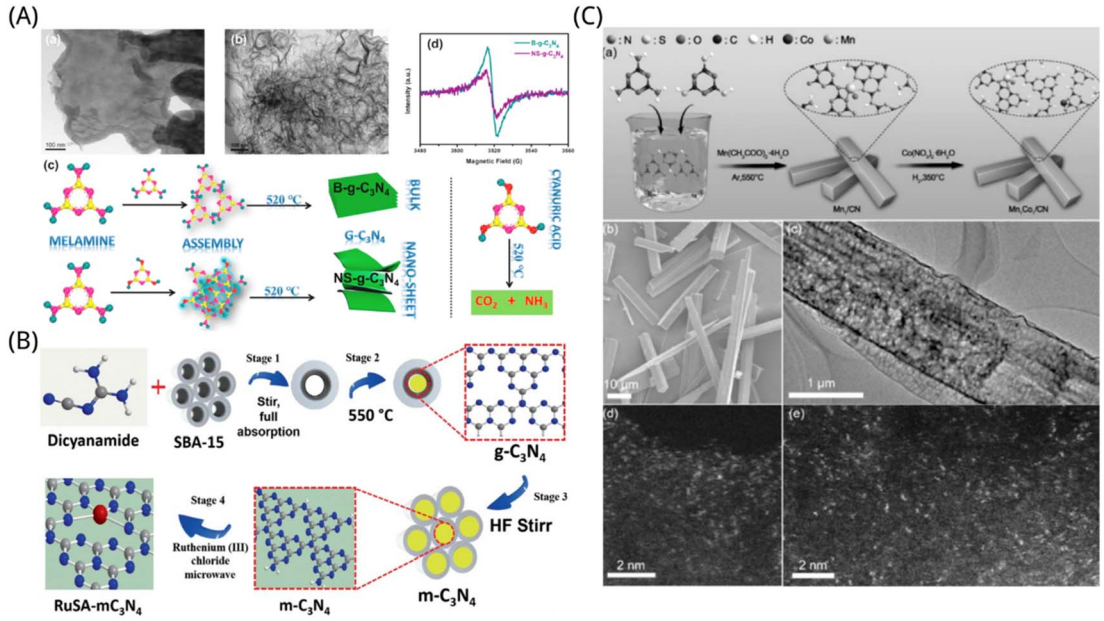

Fig. 7 (A) TEM pictures of (a) B-g-C_3N_4 and (b) NS-g-C_3N_4. (c) The steps involved in synthesizing B-g-C_3N_4 and NS-g-C_3N_4. (d) The EPR spectrogram of B-g-C_3N_4 and NS-g-C_3N_4.[183] Reproduced with permission. Copyright 2021, Elsevier Inc. (B) Schematic diagram of the synthetic procedure for a ruthenium single atom on mesoporous C_3N_4. (RuSA-mC_3N_4: Ruthenium single atom; HF: Hydrofluoric acid; mC_3N_4: mesoporous carbon nitride; SBA-15: template.)[188] Reproduced with permission. Copyright 2021, Wiley-VCH GmbH. (C) (a) Preparation of the Mn_1Co_1/CN catalyst. (b) SEM and (c) TEM diagrams of Mn_1Co_1/CN. AC HAADF-STEM diagram of (d) Mn_1/CN and (e) Mn_1Co_1/CN.[192] Reproduced with permission. Copyright 2022, Wiley-VCH GmbH.

For the purpose of increasing catalytic activity, stability and selectivity of g-C_3N_4 photocatalysts, scientists have often used single atoms decorations for refinement. Utilizing space-constrained single atom Fe and K ions, the graphitic carbon nitride (FeN_4/K-g-C_3N_4) fabricated by Cheng *et al.* demonstrated remarkable performance and selectivity for the photocatalytic CO_2 reduction process. The g-C_3N_4 layer's single atom of Fe forms a connection with its four neighboring N atoms, acting as the centre of activity for the capture and revitalization of CO_2 molecules. In addition, the alkali metal K ions may efficiently enhance segregation and transference, which together with the spatial confinement of the single atom Fe and K ions in g-C_3N_4, promotes photocatalytic performance and selectivity of CO_2 conversion to CO. The conversion rate of CO_2 to CO can reach 20.00 μmol g^{-1} h^{-1} with a selectivity close to 100%, which outperforms pure g-C_3N_4 by a factor of more than ten.[185] Zhao *et al.* further demonstrated the contribution of single-atom Fe to catalytic activity. They used density flooding theory (DFT) and time-dependent DFT (TDDFT) approaches, combined with experimental and computer-based mechanisms, to find out more about the photoreduction of CO_2 with H_2O that is facilitated by single-atom Fe-supported graphitic nitrides (g-C_3N_4) and to learn more about the function of single-atom Fe in g-C_3N_4. It was found that in the absence of the Fe atom, the speed-limiting step of the hydrogen bonding compound is the cleavage of the C–O bond in the COOH radical throughout the CO_2RR process, involving both photophysical and photochemical reactions. In addition to activating CO_2 in its ground state and increasing the rate constant of the restricting step in the photophysical reaction, the existence of the Fe atom also serves as a catalytically active centre, decreasing the restriction of the reaction for the cleavage of the C–O bond in COOH* in the photochemical process, thus improving photocatalytic activity.[186] Cheng *et al.* ligated single-atom site Ni on porous multilayers of g-C_3N_4 (*i.e.* Ni_5–CN) synthesized from the bottom up by a self-limiting approach and defined an unsaturated edge-limiting strategy. The few isolated Ni clusters in this Ni_5–CN system are dispersed on the edges of g-C_3N_4, allowing non-edge single-atom site Ni species to be immobilized and obtaining a substantial density of single-atom active sites. The advantages in N–Ni–N combinatorial link and surface carrier transference are promoted by the cationic linkage environment of the monoatomic Ni centre generated by doping Ni–N into the primary bonding shell. The Ni_5–CN system had significant photocatalytic performance for CO_2 reduction, with a CO production rate of 8.6 μmol g^{-1} h^{-1} beneath visual light, which was 7.8-fold more than the pure porous several-layer g-C_3N_4 system (*i.e.* CN, 1.1 μmol g^{-1} h^{-1}).[187] In order to achieve photocatalytic CO_2 reduction to methanol fuel utilizing water as an electron carrier and reaching an output of cat. 1500 μmol g^{-1} in 6 hours of response, Sharma *et al.* produced RuSA-mC_3N_4 photoactive catalysts by an innovative single-atom synthesis approach with single ruthenium atoms dispersed on a granular carbon nitride surface, as shown in Fig. 7B. The analysis by EXAFS absorption spectroscopy revealed that the Ru–N/C intercalation in the initial ligand shell layer formed a cationic ligand environment with a single atomic ruthenium centre, realizing a synergistic effect of N–Ru–N linkage and charge

transfer on interface. The coupling of Ru with NC sites boosts the amount of electrons transferred and charge distribution on Ru, lowering the photo-carrier transference obstacle and improving the photocatalytic performance of RuSA-mC_3N_4, which makes the average carrier life of RuSA-mC_3N_4 system longer than that of m-C_3N_4.[188] Zhang *et al.* improved the catalytic performance for CO_2 in photochemistry by embedding single cobalt(II) sites on g-C_3N_4, resulting in CO yields of up to 464.1 μmol g^{-1} h^{-1}, which are 3 and 222-fold higher than when employing Co-MOF and $CoCl_2$ as the cobalt source, correspondingly. This was accomplished by pyrolyzing ultrathin cobalt metal organic framework (MOF) nanosheets (also known as metal organic layers; MOLs) in the process of forming g-C_3N_4. When g-C_3N_4 is being formed, Co(II) sites may be evenly and atomic scale disseminated over its surface because of the confinement impact of the MOF matrix and the tight engagement of the metal organic layer with the g-C_3N_4 predecessor.[189]

It has been demonstrated that a novel method for promoting multiphase processes is single-atom photocatalysis. Numerous single-atom metal species exist, each with unique functions. However, a significant obstacle still exists in the integration of representational benefits into dual single-atom photocatalysis. The catalytic performance of dual single-atom catalysts can be improved by combining their complementary functionalities and synergistic effects. Chen *et al.* synthesized a composite of rare earth single atom La onto carbon nitride. The La–N charge-transfer bridge was used as the active centre of the photocatalytic CO_2 reduction reaction, thus promoting the activation of CO_2, rapid generation of COOH* and desorption of CO, achieving a remarkable CO generation rate of 92 μmol g^{-1} h^{-1} and a CO selectivity of 80.3%, which is superior to the majority of g-C_3N_4-based photocatalytic CO_2 reduction approaches. Moreover, the rate of CO generation remained nearly constant under five cycles of 20 hours of light, showing a more robust stability.[190] Cheng *et al.* developed diatomic catalysts loaded on conjugated porous carbon nitride polymers featuring cobalt (Co) and ruthenium (Ru) functionalities for efficient photocatalytic CO_2 reduction. During CO_2 photoreduction, the active Co site promotes dynamic charge transfer and the Ru site promotes selective CO_2 surface binding interactions. The association of particular atomic properties and the synergy between Co and Ru leads to a excellent photocatalytic CO_2 reduction with a respective apparent quantum efficiency (AQE) of 2.8% at 385 nm, as well as a high turnover number (TON) of over 200 in the absence of any added sacrificial agent.[191] Inspired by natural photosynthetic systems, Ou *et al.* created a bimetallic single-atom active site photocatalyst with Mn and Co single atoms, as shown in Fig. 7C, with two compatible Mn and Co active centres (Mn_1Co_1/CN) on carbon nitride (CN). The placement of Mn and Co bimetallic single atoms on CN as redox sites successfully improves hole–electron segregation and energy transfer by taking advantage of the synergistic impact of the atomic active centres. The Mn_1Co_1/CN photocatalyst showed excellent catalytic performance in the conversion of CO_2 to CO with a CO output of 47 μmol g^{-1} h^{-1}, significantly higher than that of the corresponding monometallic active centre photocatalyst.[192]

Although the catalytic performance and selectivity of the g-C_3N_4-based single-atom photocatalysts have been improved, their photocatalytic efficiency for CO_2 reduction still falls short of expectations. Moreover, the modified materials mostly contain precious metals, so the high cost and complicated fabrication processes are major obstacles to practical applications. Therefore, the in-depth design and fabrication of high-efficiency and inexpensive single-atom photocatalysts based on g-C_3N_4 for CO_2 conversion is still to be explored.

MOFs

Because MOFs are porous, there is a large specific surface area available for reactions. As catalytic active sites, the metal centres are evenly dispersed across the materials' interior and exterior surfaces, giving them numerous metal active sites and strong CO_2 adsorption. The metal centres and ligands create a distinctive energy band structure through electron structure matching, which is suitable for light energy absorption and transfer. Furthermore, pore channel binding results in effects which including space-limited and charge-limited domains, optimization of process intermediates, and selectivity.[193,194] Coupled with the high affinity of MOFs for CO_2 facilitates the interaction of reactants and catalysts, advancing the reaction to proceed efficiently. In addition, MOFs materials can regulate of the electronic structure of the active centre by coupling with other materials to extend the carrier lifetime and improve the utilization efficiency, giving them a unique competitive advantage in the photocatalytic CO_2 reduction process.

By including coordinated unsaturated single atoms into the MOFs matrix, the modular optimization of MOFs is accomplished. This allows the newly created MOFs to effectively and selectively absorb and photolyze CO_2 when exposed to visible light. Zhang *et al.* found that the inclusion of a single Co atom in MOFs can significantly enhance the efficiency of the porphyrin unit's ability to separate electrons from holes and can also encourage the directional migration of photogenerated excitons from the porphyrin to the catalytic Co centre, thereby providing long-lasting electrons for the conversion of CO_2 molecules immobilized in the Co centre. The porphyrin MOFs consisting of atomic scale scattered catalytic centres demonstrated dramatically improved photocatalytic CO_2 reduction that is equivalent to 3.13 times of CO precipitation rate (200.6 μmol g^{-1} h^{-1}) and 5.93 times of CH_4 production rate (36.67 μmol g^{-1} h^{-1}) in comparison to the parent MOFs, as shown in Fig. 8A.[43] The synthesis of photocatalysts from dilute metal elements and the efficient reduction of CO_2 is a difficult yet extremely appealing technique for scientists. Wang *et al.* created an indium-porphyrin structure, In(H_2-TCPP)$_{(1-n)}$[Fe(TCPP)(H_2O)]$_{(1-n)}$[DEA]$_{(1-n)}$ (In-Fe$_n$TCPP-MOF; H_2TCPP = tetrakis (4-benzoic acid) porphyrin; DEA = diethylamine),[195] as shown in Fig. 8B, for high-performance conversion of CO_2 to CO powered by visible light. Its porphyrin ring-supported iron centre is the effective active site to absorb electrons from photoexcited MOFs so as to facilitate CO_2 reduction. A 24 hour photocatalytic process with excellent CO selectivity (approximately 99.5%) may obtain a high CO output of 3469 μmol g^{-1}. Compared

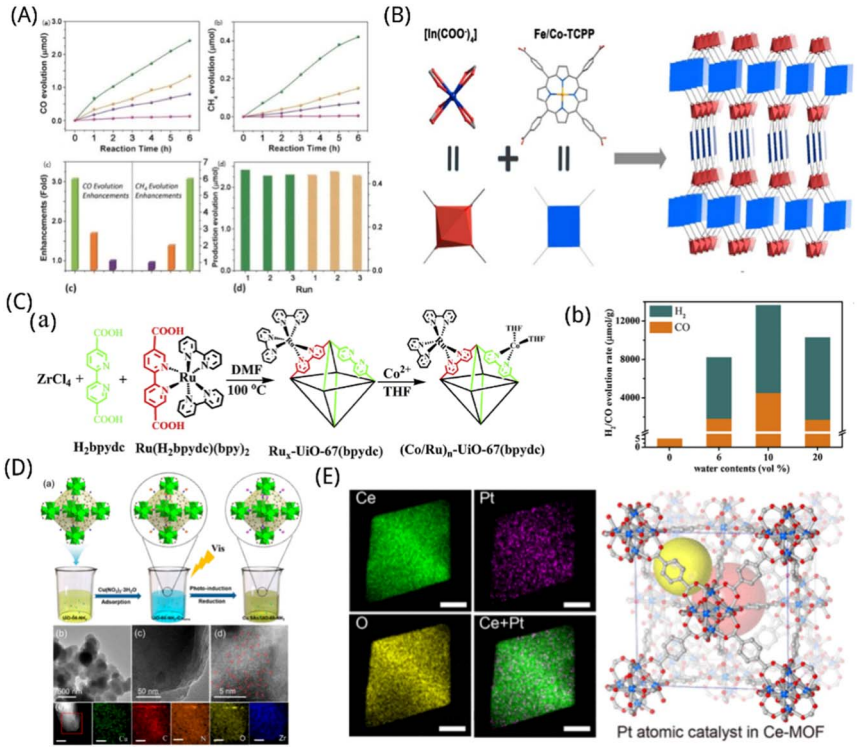

Fig. 8 (A) Time-dependent evolution of (a) CO and (b) CH_4 on MOF-525-Co (green), MOF-525-Zn (orange), MOF-525 (purple) photocatalysts and H_6TCPP ligands (pink). (c) Enhanced production evolution on MOF-525-Co (green), MOF-525-Zn (orange) and MOF-525-Zn (purple). (d) Yields of CO (green) and CH_4 (orange) production on MOF-525-Co photocatalyst as a measure of cycle reproducibility.[43] Reproduced with permission. Copyright 2016, Wiley-VCH Verlag GmbH & Co. KGaA, Weinheim. (B) Synthesis and structure of the In–Fe/CoTCPP-MOFs.[195] Reproduced with permission. Copyright 2020, American Chemical. Society. (C) (a) Schematic diagram of the synthesis of $(Co/Ru)_n$-UiO-67(bpydc); (b) comparison of H_2/CO evolution rate with different water contents.[198] Reproduced with permission. Copyright 2019, Elsevier B.V. (D) (a) The synthesis procedure of Cu SAs/UiO-66-NH_2 photocatalyst. C (gray), O (red), Zr–O clusters (green), N (blue), Cu ions (orange), and Cu SAs (purple). (b) TEM and (c) HRTEM of Cu SAs/UiO-66-NH_2. (d) Corrected STEM images of Cu SAs/UiO-66-NH_2. Cu SAs were marked with red circles. (e) EDS profiles of Cu SAs/UiO-66-NH_2.[200] Reproduced with permission. Copyright 2020, American Chemical Society. (E) Elemental mappings of Ce, Pt, O, and overlay of Ce and Pt in the Pt–SA–Ce–MOF catalyst and two types of pores in the C-MOF structure (indicated by two large yellow and red spheres).[98] Reproduced with permission. Copyright 2020, American Chemical Society.

to its cobalt counterpart or indium-based MOFs without iron, its activity is significantly greater.

It is well documented that establishing functional groupings into the skeleton of UiO series MOFs is simple and easy, and can be achieved either directly by using functionalized ligands as starting ligands, or by post-synthetic modification and replacement, with the topology of the final product remaining unchanged. These features make the UiO series MOFs have a lot of promise for use in gas separation, CO_2 capture and catalysis.[196,197] One of the environmentally friendly methods for turning CO_2 recycling into products with additional value is the photocatalytic reduction of CO_2 to syngas (CO and H_2). Utilizing a single central catalyst, Liu *et al.* created a straightforward and efficient two-step self-assembly procedure to functionalize phosphorescent metal–organic frameworks. The generated $(Co/Ru)_n$-UiO-67(bpydc) provided the molecular platform for the rapid injection of multiple electrons from photosensitizers (PSs) into the Co-catalyst, resulting in the efficient production of syngas from the MOF-based compound photocatalyst in 16 hours with a production of 13 600 μmol g^{-1} (H_2 : CO = 2 : 1), which is 29.2 times higher than its homogeneous counterpart. Moreover, through carefully controlling the PS/catalyst molar ratio in the MOFs platform as well as the content of H_2O in the photocatalytic system, the H_2/CO ratio could be successfully regulated, as shown in Fig. 8C.[198] UiO-66 is a class of MOFs material with the chemical formula $Zr_6O_4(OH)_4(CO_2)_{12}$, which was discovered and prepared by Cavka *et al.* in 2008. Due to its good hydrothermal stability, UiO-66 offers a variety of uses for gas adsorption and separation, especially in CO_2 capture, which has been studied in a variety of investigations by scholars.[197] Cmarik *et al.* explored the study of different functional groups on gas adsorption properties and found that UiO-66-NH_2 has great potential for CO_2 adsorption and separation because of the powerful interaction between polar functional group aminos and CO_2 as well as the properties of its own structural dimensions.[199] Wang *et al.* achieved the establishment of Cu single atoms on UiO-66-NH_2 carriers (Cu SAs/UiO-66-NH_2) by a photoinduced method, as shown in Fig. 8D, which greatly facilitated the photoreduction of CO_2 to liquid fuels with conversion rates of 5.33 and 4.22 μmol g^{-1} h^{-1} for CH_3OH and CH_3CH_2OH, respectively, with the superior performance than the pristine UiO-66-NH_2 and Cu nanoparticles/UiO-66-NH_2 composites. This was owing to the addition of Cu SAs to UiO-66-NH_2, which considerably aided CO_2 conversion to CHO* and

CO* intermediates, leading to the high selectivity for CH_3OH and CH_3CH_2OH.[200] Chu *et al.* presented a photo-induced reduction method for producing catalysts by attaching single atom Zn on UiO-66-NH_2. Moreover, the low-liganded Zn–N_2 site can greatly facilitate the synthesis of COOH*, which is the restrictive step in the production of CO_2, making UiO-66-NH_2-0.7Zn SAs have exceptional capacity in converting CO_2 into CO. Compared with the original UiO-66-NH_2 in the lack of the photosensitizer or hole sacrificial agent, its performance under ultraviolet-visible light is improved by about 5 times.[201] The outcomes of this study open up new possibilities for the production of highly effective photocatalysts with single-atom sites for photocatalytic CO_2 conversion.

However, the poor porosity of the support structure, the poor affinity of SAs to the support, and the high-temperature synthesis led to bottlenecks in the practical utilization of SAs, such as high manufacturing expense, poor catalytic performance, and low metal atom usage. To achieve higher catalytic efficiency and atom utilization efficiency, it is necessary to synthesize SAs in a scalable, low-energy manner that closely matches the atomic scale planned 3D nanostructures. Guo *et al.* used a low-expense ceramic MOF (Ce-MOF) with tailored flaws spanning porous and crystalline structures to produce a simple synthesis approach. The SA(Pt) produced by low-temperature photoreduction could be encased in the Ce-MOF flaws. The conjugated catalyst weighing 0.12 wt% showed 100% CO_2 conversion at a low temperature of 150 °C because of the uniform dispersion and the distinctive electronic hybridization with Ce-MOF. The amount of platinum consumed is only 10% of that consumed by the most advanced catalysts under the same conditions and has high stability, as shown in Fig. 8E, making it the current catalyst with the highest recorded efficiency.[98] Gas permeable metal–organic framework membranes can alter the electronic structure and catalytic characteristics of metal single atoms to promote diffusion, activation, and reduction of gas molecules (*e.g.*, carbon dioxide) and generate liquid fuels beneath visible illumination in the mild circumstances. Hao *et al.* found that porous metal–organic framework membranes embellished with metal single atoms could facilitate the photoreduction of CO_2 and O_2 at the high flux gas–solid interface. Using Ir SAs as active centres, defective engineered MOFs (*e.g.*, activated NH_2-UiO-66) particles may convert CO_2 to HCOOH with an apparent quantum efficiency (AQE) of 2.51% at the gas–liquid–solid interface of the reaction at 420 nm. The gas-permeable SA/MOFs membrane could directly convert moist CO_2 gas to HCOOH with high HCOOH selectivity due to the promotion of gas diffusion at the porous gas–solid interface, with a significant increase in AQE of 15.76% at 420 nm.[202] By adding structural flaws to the MOFs framework, the interatomic distance among metal sites can be extended band the aggregation of metals can be inhibited, thus increasing the yield of SACs.

By modulating the MOFs structure and defects, scientists have made photocatalysts based on MOFs materials more qualified contenders for the efficient fabrication of single-atom photocatalysts. However, the stability, cost and many uncertainties of MOFs-based materials are still a concern when put into industrial production.

Conclusions

In the paper, we succinctly make a summary about the research and promotion of new photocatalysts for CO_2 reduction from four aspects: the mechanism of the photocatalytic CO_2 reduction process, the preparation of single-atom catalysts, advantages and disadvantages of single-atom catalysts and their applications which show good promise in photocatalysis. At this stage, research on photocatalytic CO_2 conversion is still in its infancy, and its solar energy conversion efficiency has certain limitations, and still faces many challenges in research and application.

(1) Since single-atom catalysts have a low density of unsaturated active centres, researchers have mostly used highly loaded metal single-atom catalysts to raise the density of photocatalytic electron pumps and photocatalytic active centres. However, most metal single-atom catalysts have a large surface free energy, such that they are prone to agglomeration thus affecting catalytic activity and efficiency. Therefore, researchers have further modified the supporting semiconductor materials and anchored the isolated sites to reduce the agglomeration phenomenon to a certain extent, but it still needs to find more efficient, economical and workable methods to improve the stability of single-atom photocatalysts.

(2) The selectivity and activity of CO_2 reduction remain to be enhanced. Single-atom photocatalysts for CO_2 reduction remain not widely used due to their low stability and catalytic activity.

(3) The lack of in-depth comprehension of the synthesis and catalytic mechanism of single-atom catalysts, and lacking an intuitive way to characterize them, has hindered the study of the synthesis process-structure–property relationship of single atom-catalysts.

Given the aforementioned difficulties, in purpose to promote the maturation of single atom photocatalytic CO_2 reduction technology and its widespread use in production, we must methodically analyse the findings of previous studies and investigate the principle of photocatalytic processes to fill theoretical gaps and promote the creation of effective and affordable novel photocatalytic materials, which can actively promote the cross-fertilization of photocatalysis with other fields and explore the application and development of efficient and stable photocatalyst in more fields. As technology and science advance and the deep understanding of the "carbon peaking and carbon neutrality" theory grows, photocatalytic CO_2 reduction technology will move towards a more mature and broader field.

Author contributions

Miss Wanyu Hu: writing – original draft and conceptualization. Prof. Haiyue Yang: supervision and writing – review & editing. Prof. Chengyu Wang: resources and supervision.

Conflicts of interest

The authors declare that they have no known competing financial interests or personal relationships that could have appeared to influence the work reported in this paper.

Acknowledgements

This project was supported by China Postdoctoral Science Foundation (grant no. 2021M700736) and Postdoctoral Foundation of Heilongjiang (grant no. LBH-Z21089).

Notes and references

1 S. Hernandez-Aldave and E. Andreoli, *Catal. Sci. Technol.*, 2022, **12**, 3412–3420.
2 M. I. Alam, R. Cheula, G. Moroni, L. Nardi and M. Maestri, *Catal. Sci. Technol.*, 2021, **11**, 6601–6629.
3 C. Gao, J. Low, R. Long, T. Kong, J. Zhu and Y. Xiong, *Chem. Rev.*, 2020, **120**, 12175–12216.
4 M. S. Dresselhaus and I. L. Thomas, *Nature*, 2001, **414**, 332–337.
5 N. S. Lewis and D. G. Nocera, *Proceedings of the National Academy of Sciences*, 2006, **103**, 15729–15735.
6 W. Dessie, X. Luo, M. Wang, L. Feng, Y. Liao, Z. Wang, Z. Yong and Z. Qin, *Appl. Microbiol. Biotechnol.*, 2020, **104**, 4757–4770.
7 L. Jiang, Q. Yang, Z. Xia, X. Yu, M. Zhao, Q. Shi and Q. Yu, *RSC Adv.*, 2023, **13**, 5833–5850.
8 H. Li, P. H. Opgenorth, D. G. Wernick, S. Rogers, T.-Y. Wu, W. Higashide, P. Malati, Y.-X. Huo, K. M. Cho and J. C. Liao, *Science*, 2012, **335**, 1596.
9 S. Chen, K. Li, H. Liu, J. Zhang and T. Peng, *Catal. Sci. Technol.*, 2022, **12**, 1637–1650.
10 M. Irshad, Q. tul Ain, M. Zaman, M. Z. Aslam, N. Kousar, M. Asim, M. Rafique, K. Siraj, A. N. Tabish and M. Usman, *RSC Adv.*, 2022, **12**, 7009–7039.
11 Z.-H. Xue, D. Luan, H. Zhang and X. W. D. Lou, *Joule*, 2022, **6**, 92–133.
12 Y. Lu, Z. Zhang, H. Wang and Y. Wang, *Appl. Catal., B*, 2021, **292**, 120162.
13 S. Wang, G. Li and C. Fang, *Renewable Sustainable Energy Rev.*, 2018, **81**, 2144–2159.
14 S. Davis, D. Nugegoda, J. Tropp, J. D. Azoulay and J. H. Delcamp, *MRS Commun.*, 2020, **10**, 252–258.
15 X. Guan, S. S. Mao and S. Shen, *ChemNanoMat*, 2021, **7**, 873–880.
16 X. Chang, T. Wang and J. Gong, *Energy Environ. Sci.*, 2016, **9**, 2177–2196.
17 Y. Tamaki, T. Morimoto, K. Koike and O. Ishitani, *Proc. Natl. Acad. Sci. U. S. A.*, 2012, **109**, 15673–15678.
18 R. Kuriki, K. Sekizawa, O. Ishitani and K. Maeda, *Angew. Chem., Int. Ed.*, 2015, **54**, 2406–2409.
19 H. Pan and M. D. Heagy, *Nanomaterials*, 2020, **10**, 2422.
20 M. Zhang, X. Wang, X. Qi, H. Guo, L. Liu, Q. Zhao and W. Cui, *J. Catal.*, 2022, **413**, 31–47.
21 S. Wang and X. Wang, *Appl. Catal., B*, 2015, **162**, 494–500.
22 K. Niu, Y. Xu, H. Wang, R. Ye, H. L. Xin, F. Lin, C. Tian, Y. Lum, K. C. Bustillo, M. M. Doeff, M. T. M. Koper, J. Ager, R. Xu and H. Zheng, *Sci. Adv.*, 2017, **3**, e1700921.
23 X. Xiong, C. Mao, Z. Yang, Q. Zhang, G. I. N. Waterhouse, L. Gu and T. Zhang, *Adv. Energy Mater.*, 2020, **10**, 2002928.
24 X. Li, Y. Sun, J. Xu, Y. Shao, J. Wu, X. Xu, Y. Pan, H. Ju, J. Zhu and Y. Xie, *Nat. Energy*, 2019, **4**, 690–699.
25 R. Wang, J. Shen, K. Sun, H. Tang and Q. Liu, *Appl. Surf. Sci.*, 2019, **493**, 1142–1149.
26 K. Jiang, L. Zhu, Z. Wang, K. Liu, H. Li, J. Hu, H. Pan, J. Fu, N. Zhang, X. Qiu and M. Liu, *Appl. Surf. Sci.*, 2020, **508**, 145173.
27 Y. Wang, H. Huang, Z. Zhang, C. Wang, Y. Yang, Q. Li and D. Xu, *Appl. Catal., B*, 2021, **282**, 119570.
28 W. Li, D.-K. Ma, X. Hu, F. Gou, X. Yang, W. MacSwain, C. Qi and W. Zheng, *J. Catal.*, 2022, **415**, 77–86.
29 M. R. U. D. Biswas, A. Ali, K. Y. Cho and W.-C. Oh, *Ultrason. Sonochem.*, 2018, **42**, 738–746.
30 A. Lais, M. A. Gondal, M. A. Dastageer and F. F. Al-Adel, *Int. J. Energy Res.*, 2018, **42**, 2031–2049.
31 S. Navarro-Jaen, M. Virginie, J. Bonin, M. Robert, R. Wojcieszak and A. Y. Khodakov, *Nat. Rev. Chem.*, 2021, **5**, 564–579.
32 Y. Zhang, L. Zheng, J. Jia, K. Li, T. Zhang and H. Yu, *Colloids Surf., A*, 2022, 639.
33 J. Ran, M. Jaroniec and S.-Z. Qiao, *Adv. Mater.*, 2018, **30**, 1704649.
34 H. Tong, S. Ouyang, Y. Bi, N. Umezawa, M. Oshikiri and J. Ye, *Adv. Mater.*, 2012, **24**, 229–251.
35 J. Fu, K. Jiang, X. Qiu, J. Yu and M. Liu, *Mater. Today*, 2020, **32**, 222–243.
36 Q. Zhang and J. Guan, *Sol. RRL*, 2020, **4**, 2000283.
37 Q. Wang, D. Zhang, Y. Chen, W.-F. Fu and X.-J. Lv, *ACS Sustainable Chem. Eng.*, 2019, **7**, 6430–6443.
38 S. Liang, C. Hao and Y. Shi, *Chemcatchem*, 2015, **7**, 2559–2567.
39 Y. Xia, M. Sayed, L. Zhang, B. Cheng and J. Yu, *Chem Catal.*, 2021, **1**, 1173–1214.
40 S. Liang, C. Hao and Y. Shi, *ChemCatChem*, 2015, **7**, 2559–2567.
41 Q. Wang and K. Domen, *Chem. Rev.*, 2020, **120**, 919–985.
42 J. Xing, J. F. Chen, Y. H. Li, W. T. Yuan, Y. Zhou, L. R. Zheng, H. F. Wang, P. Hu, Y. Wang, H. J. Zhao, Y. Wang and H. G. Yang, *Chem. - Eur. J.*, 2014, **20**, 2138–2144.
43 H. Zhang, J. Wei, J. Dong, G. Liu, L. Shi, P. An, G. Zhao, J. Kong, X. Wang, X. Meng, J. Zhang and J. Ye, *Angew. Chem., Int. Ed.*, 2016, **55**, 14308–14312.
44 W. Liu, L. Cao, W. Cheng, Y. Cao, X. Liu, W. Zhang, X. Mou, L. Jin, X. Zheng, W. Che, Q. Liu, T. Yao and S. Wei, *Angew. Chem., Int. Ed.*, 2017, **56**, 9312.
45 D. Yang, H. Yu, T. He, S. Zuo, X. Liu, H. Yang, B. Ni, H. Li, L. Gu, D. Wang and X. Wang, *Nat. Commun.*, 2019, **10**, 3844.
46 S. Bai, J. Jiang, Q. Zhang and Y. Xiong, *Chem. Soc. Rev.*, 2015, **44**, 2893–2939.
47 C. Gao, J. Wang, H. Xu and Y. Xiong, *Chem. Soc. Rev.*, 2017, **46**, 2799–2823.
48 J. Schneider, M. Matsuoka, M. Takeuchi, J. Zhang, Y. Horiuchi, M. Anpo and D. W. Bahnemann, *Chem. Rev.*, 2014, **114**, 9919–9986.
49 C. Peng, G. Reid, H. Wang and P. Hu, *J. Chem. Phys.*, 2017, **147**, 030901.

50 A. Folli, J. Z. Bloh and D. E. Macphee, *J. Electroanal. Chem.*, 2016, **780**, 367–372.
51 S. S. Tan, L. Zou and E. Hu, *Catal. Today*, 2006, **115**, 269–273.
52 M.-Q. Yang, M. Gao, M. Hong and G. W. Ho, *Adv. Mater.*, 2018, **30**, 1802894.
53 Y. Chen, Y. Liu, F. Wang, X. Guan and L. Guo, *J. Energy Chem.*, 2021, **61**, 469–488.
54 Y. Zhang, B. Xia, J. Ran, K. Davey and S. Z. Qiao, *Adv. Energy Mater.*, 2020, **10**, 1903879.
55 Y. Xia and J. Yu, *Chem*, 2020, **6**, 1039–1040.
56 X. Jiao, K. Zheng, L. Liang, X. Li, Y. Sun and Y. Xie, *Chem. Soc. Rev.*, 2020, **49**, 6592–6604.
57 C. B. Hiragond, N. S. Powar, J. Lee and S.-I. In, *Small*, 2022, **18**, 2201428.
58 N. Zheng and T. Zhang, *Natl. Sci. Rev.*, 2018, **5**, 625.
59 K. Qi, M. Chhowalla and D. Voiry, *Mater. Today*, 2020, **40**, 173–192.
60 Z. Li, S. Ji, Y. Liu, X. Cao, S. Tian, Y. Chen, Z. Niu and Y. Li, *Chem. Rev.*, 2020, **120**, 623–682.
61 Q. Xu, J. Zhang, D. Wang and Y. Li, *Chin. Chem. Lett.*, 2021, **32**, 3771–3781.
62 D. V. R. Kumar, K. Woo and J. Moon, *Nanoscale*, 2015, **7**, 17195–17210.
63 P. Chen, W. Zhang, Y. Sun and F. Dong, *Environ. Funct. Mater.*, 2022, **1**, 127–138.
64 P. Biasi, S. Sterchele, F. Bizzotto, M. Manzoli, S. Lindholm, P. Ek, J. Bobacka, J.-P. Mikkola and T. Salmi, *Catal. Today*, 2015, **246**, 207–215.
65 D. Zhao, Z. Chen, W. Yang, S. Liu, X. Zhang, Y. Yu, W.-C. Cheong, L. Zheng, F. Ren, G. Ying, X. Cao, D. Wang, Q. Peng, G. Wang and C. Chen, *J. Am. Chem. Soc.*, 2019, **141**, 4086–4093.
66 H. Xu, N. Jiang, D. Wang, L. Wang, Y. Song, Z. Chen, J. Ma and T. Zhang, *Appl. Catal., B*, 2020, **263**, 118350.
67 J. Xing, J. F. Chen, Y. H. Li, W. T. Yuan, Y. Zhou, L. R. Zheng, H. F. Wang, P. Hu, Y. Wang and H. J. Zhao, *Chem. – Eur. J.*, 2014, **20**, 2138–2144.
68 Y. Lu, C. Zhang, X. Li, A. R. Frojd, W. Xing, A. Z. Clayborne and W. Chen, *Nano Energy*, 2018, **50**, 316–322.
69 R. Lang, W. Xi, J.-C. Liu, Y.-T. Cui, T. Li, A. F. Lee, F. Chen, Y. Chen, L. Li and L. Li, *Nat. Commun.*, 2019, **10**, 234.
70 J. Lin, A. Wang, B. Qiao, X. Liu, X. Yang, X. Wang, J. Liang, J. Li, J. Liu and T. Zhang, *J. Am. Chem. Soc.*, 2013, **135**, 15314–15317.
71 J. Ding, M. Fan, Q. Zhong and A. G. Russell, *Appl. Catal., B*, 2018, **232**, 348–354.
72 J. A. Schwarz, C. Contescu and A. Contescu, *Chem. Rev.*, 1995, **95**, 477–510.
73 S. Sun, G. Zhang, N. Gauquelin, N. Chen, J. Zhou, S. Yang, W. Chen, X. Meng, D. Geng, M. N. Banis, R. Li, S. Ye, S. Knights, G. A. Botton, T.-K. Sham and X. Sun, *Sci. Rep.*, 2013, **3**, 1775.
74 M. Leskela and M. Ritala, *Angew. Chem., Int. Ed.*, 2003, **42**, 5548–5554.
75 X. Ye, H. Wang, Y. Lin, X. Liu, L. Cao, J. Gu and J. Lu, *Nano Res.*, 2019, **12**, 1401–1409.
76 T. J. Gorey, B. Zandkarimi, G. Li, E. T. Baxter, A. N. Alexandrova and S. L. Anderson, *J. Phys. Chem. C*, 2019, **123**, 16194–16209.
77 L. Zhang, M. R. Ball, K. R. Rivera-Dones, S.-c. Wang, T. F. Kuech, G. W. Huber, I. Hermans and J. A. Dumesic, *ACS Catal.*, 2020, **10**, 365–374.
78 B. Qiao, A. Wang, X. Yang, L. F. Allard, Z. Jiang, Y. Cui, J. Liu, J. Li and T. Zhang, *Nat. Chem.*, 2011, **3**, 634–641.
79 J. D. Kistler, N. Chotigkrai, P. Xu, B. Enderle, P. Praserthdam, C. Y. Chen, N. D. Browning and B. C. Gates, *Angew. Chem., Int. Ed.*, 2014, **53**, 8904–8907.
80 X.-K. Gu, B. Qiao, C.-Q. Huang, W.-C. Ding, K. Sun, E. Zhan, T. Zhang, J. Liu and W.-X. Li, *ACS Catal.*, 2014, **4**, 3886–3890.
81 L. Yang, L. Shi, D. Wang, Y. Lv and D. Cao, *Nano Energy*, 2018, **50**, 691–698.
82 J. Kim, C. W. Roh, S. K. Sahoo, S. Yang, J. Bae, J. W. Han and H. Lee, *Adv. Energy Mater.*, 2018, **8**, 1701476.
83 X. Zeng, J. Shui, X. Liu, Q. Liu, Y. Li, J. Shang, L. Zheng and R. Yu, *Adv. Energy Mater.*, 2018, **8**, 1701345.
84 J. Li, Q. Guan, H. Wu, W. Liu, Y. Lin, Z. Sun, X. Ye, X. Zheng, H. Pan, J. Zhu, S. Chen, W. Zhang, S. Wei and J. Lu, *J. Am. Chem. Soc.*, 2019, **141**, 14515–14519.
85 Z. Song, Y.-N. Zhu, H. Liu, M. N. Banis, L. Zhang, J. Li, K. Doyle-Davis, R. Li, T.-K. Sham, L. Yang, A. Young, G. A. Botton, L.-M. Liu and X. Sun, *Small*, 2020, **16**, 2003096.
86 M. J. Huelsey, B. Zhang, Z. Ma, H. Asakura, D. A. Do, W. Chen, T. Tanaka, P. Zhang, Z. Wu and N. Yan, *Nat. Commun.*, 2019, **10**, 1330.
87 A. Jan, J. Shin, J. Ahn, S. Yang, K. J. Yoon, J.-W. Son, H. Kim, J.-H. Lee and H.-I. Ji, *RSC Adv.*, 2019, **9**, 27002–27012.
88 Z. Jiang, X. Feng, J. Deng, C. He, M. Douthwaite, Y. Yu, J. Liu, Z. Hao and Z. Zhao, *Adv. Funct. Mater.*, 2019, **29**, 1902041.
89 X. Li, W. Bi, L. Zhang, S. Tao, W. Chu, Q. Zhang, Y. Luo, C. Wu and Y. Xie, *Adv. Mater.*, 2016, **28**, 2427–2431.
90 A. V. Rassolov, I. S. Mashkovsky, G. O. Bragina, G. N. Baeva, P. V. Markov, N. S. Smirnova, J. Wärnå, A. Y. Stakheev and D. Y. Murzin, *Mol. Catal.*, 2021, **506**, 111550.
91 Y. Su, K. Fu, Y. Zheng, N. Ji, C. Song, D. Ma, X. Lu, R. Han and Q. Liu, *Appl. Catal., B*, 2021, **288**, 119980.
92 R. Lang, T. Li, D. Matsumura, S. Miao, Y. Ren, Y. T. Cui, Y. Tan, B. Qiao, L. Li and A. Wang, *Angew. Chem., Int. Ed.*, 2016, **55**, 16054–16058.
93 K. Jiang, S. Siahrostami, T. Zheng, Y. Hu, S. Hwang, E. Stavitski, Y. Peng, J. Dynes, M. Gangisetty and D. Su, *Energy Environ. Sci.*, 2018, **11**, 893–903.
94 Y. Cheng, S. Zhao, H. Li, S. He, J.-P. Veder, B. Johannessen, J. Xiao, S. Lu, J. Pan and M. F. Chisholm, *Appl. Catal., B*, 2019, **243**, 294–303.
95 X. Hai, S. Xi, S. Mitchell, K. Harrath, H. Xu, D. F. Akl, D. Kong, J. Li, Z. Li and T. Sun, *Nat. Nanotechnol.*, 2022, **17**, 174–181.
96 T. Gan, Y. Liu, Q. He, H. Zhang, X. He and H. Ji, *ACS Sustainable Chem. Eng.*, 2020, **8**, 8692–8699.
97 J. Hu, W. Ma, Y. Pan, Z. Cheng, S. Yu, J. Gao, Z. Zhang, C. Wan and C. Qiu, *Chemosphere*, 2021, **276**, 130170.

98 S. Guo, Y. Zhao, C. Wang, H. Jiang and G. J. Cheng, *ACS Appl. Mater. Interfaces*, 2020, **12**, 26068–26075.
99 Z. Huang, T. Ban, Y. Zhang, L. Wang, S. Guo, C.-R. Chang and G. Jing, *Appl. Catal., B*, 2021, **283**, 119625.
100 S.-G. Han, D.-D. Ma, S.-H. Zhou, K. Zhang, W.-B. Wei, Y. Du, X.-T. Wu, Q. Xu, R. Zou and Q.-L. Zhu, *Appl. Catal., B*, 2021, **283**, 119591.
101 M. Xiao, L. Zhang, B. Luo, M. Lyu, Z. Wang, H. Huang, S. Wang, A. Du and L. Wang, *Angew. Chem.*, 2020, **132**, 7297–7301.
102 Y. Cao, H. Peng, S. Chu, Y. Tang, C. Huang, Z. Wang, F. Liu, J. Wu, B. Shan and R. Chen, *Chem. Eng. J.*, 2021, **420**, 129713.
103 J. Shan, J. Liu, M. Li, S. Lustig, S. Lee and M. Flytzani-Stephanopoulos, *Appl. Catal., B*, 2018, **226**, 534–543.
104 W.-H. Lai, Z. Miao, Y.-X. Wang, J.-Z. Wang and S.-L. Chou, *Adv. Energy Mater.*, 2019, **9**, 2002473.
105 J. S. Kim, B. Kim, H. Kim and K. Kang, *Adv. Energy Mater.*, 2018, **8**, 1702774.
106 E. J. Jang, J. Lee, D. G. Oh and J. H. Kwak, *ACS Catal.*, 2021, **11**, 5894–5905.
107 U. Kerketta, A. B. Tesler and P. Schmuki, *Catalysts*, 2022, **12**, 1223.
108 D. Liu, Q. He, S. Ding and L. Song, *Adv. Energy Mater.*, 2020, **10**, 2001482.
109 F. Zaera, *Chem. Soc. Rev.*, 2013, **42**, 2746–2762.
110 L. Lin, T. Hisatomi, S. Chen, T. Takata and K. Domen, *Trends Chem.*, 2020, **2**, 813–824.
111 Y. Liu, Z. Liu, D. Huang, M. Cheng, G. Zeng, C. Lai, C. Zhang, C. Zhou, W. Wang, D. Jiang, H. Wang and B. Shao, *Coord. Chem. Rev.*, 2019, **388**, 63–78.
112 X.-F. Yang, A. Wang, B. Qiao, J. Li, J. Liu and T. Zhang, *Acc. Chem. Res.*, 2013, **46**, 1740–1748.
113 J. Liu, H. Wu, F. Li, X. Feng, P. Zhang and L. Gao, *Adv. Sustainable Syst.*, 2020, **4**, 2000151.
114 H. Zhang, G. Liu, L. Shi and J. Ye, *Adv. Energy Mater.*, 2018, **8**, 1701343.
115 A. Wang, J. Li and T. Zhang, *Nat. Rev. Chem.*, 2018, **2**, 65–81.
116 T. Cui, L. Li, C. Ye, X. Li, C. Liu, S. Zhu, W. Chen and D. Wang, *Adv. Funct. Mater.*, 2022, **32**, 2108381.
117 S. G. Han, D. D. Ma and Q. L. Zhu, *Small Methods*, 2021, **5**, 2100102.
118 H. He, H. H. Wang, J. Liu, X. Liu, W. Li and Y. Wang, *Molecules*, 2021, **26**, 6501.
119 Y. Zeng, E. Almatrafi, W. Xia, B. Song, W. Xiong, M. Cheng, Z. Wang, Y. Liang, G. Zeng and C. Zhou, *Coord. Chem. Rev.*, 2023, **475**, 214874.
120 R. Zheng, Z. Liu, Y. Wang, Z. Xie and M. He, *Joule*, 2022, **6**, 1148–1159.
121 T. Wang, X. Tao, X. Li, K. Zhang, S. Liu and B. Li, *Small*, 2021, **17**, 2006255.
122 L. Chen, R. R. Unocic, A. S. Hoffman, J. Hong, A. H. Braga, Z. Bao, S. R. Bare and J. Szanyi, *JACS Au*, 2021, **1**, 977–986.
123 B. Wang, H. Cai and S. Shen, *Small Methods*, 2019, **3**, 1800447.
124 S. Tu, Y. Guo, Y. Zhang, C. Hu, T. Zhang, T. Ma and H. Huang, *Adv. Funct. Mater.*, 2020, **30**, 2005158.
125 Q. Tay, P. Kanhere, C. F. Ng, S. Chen, S. Chakraborty, A. C. H. Huan, T. C. Sum, R. Ahuja and Z. Chen, *Chem. Mater.*, 2015, **27**, 4930–4933.
126 L. Zeng, C. Dai, B. Liu and C. Xue, *J. Mater. Chem. A*, 2019, **7**, 24217–24221.
127 T. Wang, F. Sun, S. Liu, G. Zhuang and B. Li, *Appl. Catal., B*, 2023, **325**, 122339.
128 N. Fu, X. Liang, Z. Li and Y. Li, *Phys. Chem. Chem. Phys.*, 2022, **24**, 17417–17438.
129 W. Qu, C. Chen, Z. Tang, H. Wen, L. Hu, D. Xia, S. Tian, H. Zhao, C. He and D. Shu, *Coord. Chem. Rev.*, 2023, **474**, 214855.
130 L. Nie, D. Mei, H. Xiong, B. Peng, Z. Ren, X. I. P. Hernandez, A. DeLaRiva, M. Wang, M. H. Engelhard, L. Kovarik, A. K. Datye and Y. Wang, *Science*, 2019, **363**, 1419–1423.
131 P. Huang, J. Huang, S. A. Pantovich, A. D. Carl, T. G. Fenton, C. A. Caputo, R. L. Grimm, A. I. Frenkel and G. Li, *J. Am. Chem. Soc.*, 2018, **140**, 16042–16047.
132 Z. Wang, J. Yang, J. Cao, W. Chen, G. Wang, F. Liao, X. Zhou, F. Zhou, R. Li and Z.-Q. Yu, *ACS Nano*, 2020, **14**, 6164–6172.
133 Y. Pan, Y. Qian, X. Zheng, S.-Q. Chu, Y. Yang, C. Ding, X. Wang, S.-H. Yu and H.-L. Jiang, *Natl. Sci. Rev.*, 2021, **8**, nwaa224.
134 J. Liu, *ACS Catal.*, 2017, **7**, 34–59.
135 T. Wang, L. Chen, C. Chen, M. Huang, Y. Huang, S. Liu and B. Li, *ACS Nano*, 2022, **16**, 2306–2318.
136 D. Zhang, Y. Li, Y. Li and S. Zhan, *SmartMat*, 2022, **3**, 417–446.
137 L. Wang, L. Huang, F. Liang, S. Liu, Y. Wang and H. Zhang, *Chin. J. Catal.*, 2017, **38**, 1528–1539.
138 H. Liu, M. Cheng, Y. Liu, J. Wang, G. Zhang, L. Li, L. Du, G. Wang, S. Yang and X. Wang, *Energy Environ. Sci.*, 2022, **15**, 3722–3749.
139 G. Wang, Y. Wu, Z. Li, Z. Lou, Q. Chen, Y. Li, D. Wang and J. Mao, *Angew. Chem., Int. Ed.*, 2023, **62**, e202218460.
140 F. Doherty, H. Wang, M. Yang and B. R. Goldsmith, *Catal. Sci. Technol.*, 2020, **10**, 5772–5791.
141 J. Guo, J. Huo, Y. Liu, W. Wu, Y. Wang, M. Wu, H. Liu and G. Wang, *Small Methods*, 2019, **3**, 1900159.
142 Y. Chen, Z. Huang, Z. Ma, J. Chen and X. Tang, *Catal. Sci. Technol.*, 2017, **7**, 4250–4258.
143 Z. Gao, Y. Meng, A. Koso, J. Mishima, B. Xie, Z. Ni and S. Xia, *Colloids Surf., A*, 2022, **648**, 129365.
144 Q. Wang, X. Y. Kong, Y. Wang, L. Wang, Y. Huang, H. Li, T. Ma and L. Ye, *ChemSusChem*, 2022, e202201514.
145 P. Liu, Y. Zhao, R. Qin, L. Gu, P. Zhang, G. Fu and N. Zheng, *Sci. Bull.*, 2018, **63**, 675–682.
146 H. Li, H.-x. Zhang, X.-l. Yan, B.-s. Xu and J.-j. Guo, *New Carbon Mater.*, 2018, **33**, 1–11.
147 J. Liu, *ChemCatChem*, 2011, **3**, 934–948.
148 T. A. Shifa and A. Vomiero, *Adv. Energy Mater.*, 2019, **9**, 1970158.
149 L. Zhang, L. Xue, B. Lin, Q. Zhao, S. Wan, Y. Wang, H. Jia and H. Xiong, *ChemSusChem*, 2022, **15**, e202102494.
150 Y. Yao, Y. Hu, H. Hu, L. Chen, M. Yu, M. Gao and S. Wang, *J. Colloid Interface Sci.*, 2019, **554**, 376–387.

151 X. Liu, W. Chen and W. Wang, *ACS Omega*, 2021, **6**, 35799–35809.
152 J. Su, R. Ge, Y. Dong, F. Hao and L. Chen, *J. Mater. Chem. A*, 2018, **6**, 14025–14042.
153 J. Gu, Y. Peng, T. Zhou, J. Ma, H. Pang and Y. Yamauchi, *Nano Res. Energy*, 2022, **1**, e9120009.
154 X. Cui, W. Li, P. Ryabchuk, K. Junge and M. Beller, *Nat. Catal.*, 2018, **1**, 385–397.
155 P. Liu, Y. Zhao, R. Qin, L. Gu, P. Zhang, G. Fu and N. Zheng, *Sci. Bull.*, 2018, **63**, 675–682.
156 Y. Z. Wang, M. Yang, Y.-M. Ding, N.-W. Li and L. Yu, *Adv. Funct. Mater.*, 2022, **32**, 2108681.
157 J. Kim, H. E. Kim and H. Lee, *ChemSusChem*, 2018, **11**, 104–113.
158 Q. Li, Q. Shao, Q. Wu, Q. Duan, Y. Li and H.-g. Wang, *Catal. Sci. Technol.*, 2018, **8**, 3572–3579.
159 P. Li, H. Wang, X. Tan, W. Hu, M. Huang, J. Shi, J. Chen, S. Liu, Z. Shi and Z. Li, *Appl. Catal., B*, 2022, **316**, 121674.
160 J. Zhang, B. Guan, X. Wu, Y. Chen, J. Guo, Z. Ma, S. Bao, X. Jiang, L. Chen and K. Shu, *Catal. Sci. Technol.*, 2023, **13**, 1932–1975.
161 Z. Shi, W. Yang, Y. Gu, T. Liao and Z. Sun, *Adv. Sci.*, 2020, **7**, 2001069.
162 L. Zhang, R. Long, Y. Zhang, D. Duan, Y. Xiong, Y. Zhang and Y. Bi, *Angew. Chem., Int. Ed.*, 2020, **59**, 6224–6229.
163 L. Jiao and H.-L. Jiang, *Chem*, 2019, **5**, 786–804.
164 C.-C. Hou, H.-F. Wang, C. Li and Q. Xu, *Energy Environ. Sci.*, 2020, **13**, 1658–1693.
165 Y.-S. Wei, M. Zhang, R. Zou and Q. Xu, *Chem. Rev.*, 2020, **120**, 12089–12174.
166 M.-L. Hu, V. Safarifard, E. Doustkhah, S. Rostamnia, A. Morsali, N. Nouruzi, S. Beheshti and K. Akhbari, *Microporous Mesoporous Mater.*, 2018, **256**, 111–127.
167 L. Hu, W. Li, L. Wang and B. Wang, *EnergyChem*, 2021, **3**, 100056.
168 Z. Xiong, Z. Lei, B. Gong, X. Chen, Y. Zhao, J. Zhang, C. Zheng and J. C. Wu, *Catal. Commun.*, 2017, **89**, 4–8.
169 T. Inoue, A. Fujishima, S. Konishi and K. Honda, *Nature*, 1979, **277**, 637–638.
170 H. S. Zakria, M. H. D. Othman, R. Kamaludin, S. H. S. A. Kadir, T. A. Kurniawan and A. Jilani, *RSC Adv.*, 2021, **11**, 6985–7014.
171 Y. Li and C.-Y. Wu, *Environ. Sci. Technol.*, 2006, **40**, 6444–6448.
172 M. A. Hossen, H. Solayman, K. H. Leong, L. C. Sim, Y. Nurashikin, A. Abd Aziz, L. Wu and M. U. Monir, *Results Eng.*, 2022, 100795.
173 H. Pan, X. Wang, Z. Xiong, M. Sun, M. Murugananthan and Y. Zhang, *Environ. Res.*, 2021, **198**, 111176.
174 Y. Yu, X. a. Dong, P. Chen, Q. Geng, H. Wang, J. Li, Y. Zhou and F. Dong, *ACS Nano*, 2021, **15**, 14453–14464.
175 H. Yin, F. Dong, D. Wang and J. Li, *ACS Catal.*, 2022, **12**, 14096–14105.
176 B.-H. Lee, E. Gong, M. Kim, S. Park, H. R. Kim, J. Lee, E. Jung, C. W. Lee, J. Bok and Y. Jung, *Energy Environ. Sci.*, 2022, **15**, 601–609.
177 Y. Feng, C. Wang, P. Cui, C. Li, B. Zhang, L. Gan, S. Zhang, X. Zhang, X. Zhou and Z. Sun, *Adv. Mater.*, 2022, **34**, 2109074.
178 C. Chen, T. Wang, K. Yan, S. Liu, Y. Zhao and B. Li, *Inorg. Chem. Front.*, 2022, **9**, 4753–4767.
179 D. Li, Y. Zhao, Y. Miao, C. Zhou, L.-P. Zhang, L.-Z. Wu and T. Zhang, *Adv. Mater.*, 2022, **34**, 2207793.
180 Q. Liu, Z.-X. Low, L. Li, A. Razmjou, K. Wang, J. Yao and H. Wang, *J. Mater. Chem. A*, 2013, **1**, 11563–11569.
181 S. Yan, Z. Li and Z. Zou, *Langmuir*, 2009, **25**, 10397–10401.
182 P. P. Singh and V. Srivastava, *RSC Adv.*, 2022, **12**, 18245–18265.
183 Y. Qin, G. Dong, L. Zhang, G. Li and T. An, *Environ. Res.*, 2021, **195**, 110880.
184 S. Liu, F. Chen, S. Li, X. Peng and Y. Xiong, *Appl. Catal., B*, 2017, **211**, 1–10.
185 X. Cheng, J. Wang, K. Zhao and Y. Bi, *Appl. Catal., B*, 2022, **316**, 121643.
186 Z. Zhao, W. Liu, Y. Shi, H. Zhang, X. Song, W. Shang and C. Hao, *Phys. Chem. Chem. Phys.*, 2021, **23**, 4690–4699.
187 L. Cheng, H. Yin, C. Cai, J. Fan and Q. Xiang, *Small*, 2020, **16**, 2002411.
188 P. Sharma, S. Kumar, O. Tomanec, M. Petr, J. Zhu Chen, J. T. Miller, R. S. Varma, M. B. Gawande and R. Zbořil, *Small*, 2021, **17**, 2006478.
189 J.-H. Zhang, W. Yang, M. Zhang, H.-J. Wang, R. Si, D.-C. Zhong and T.-B. Lu, *Nano Energy*, 2021, **80**, 105542.
190 P. Chen, B. Lei, X. a. Dong, H. Wang, J. Sheng, W. Cui, J. Li, Y. Sun, Z. Wang and F. Dong, *ACS Nano*, 2020, **14**, 15841–15852.
191 L. Cheng, X. Yue, L. Wang, D. Zhang, P. Zhang, J. Fan and Q. Xiang, *Adv. Mater.*, 2021, **33**, 2105135.
192 H. Ou, S. Ning, P. Zhu, S. Chen, A. Han, Q. Kang, Z. Hu, J. Ye, D. Wang and Y. Li, *Angew. Chem.*, 2022, **134**, e202206579.
193 X. Zeng, C. Xiao, L. Liao, Z. Tu, Z. Lai, K. Xiong and Y. Wen, *Nanomaterials*, 2022, **12**, 4049.
194 B. Smit and T. L. Maesen, *Nature*, 2008, **451**, 671–678.
195 S.-S. Wang, H.-H. Huang, M. Liu, S. Yao, S. Guo, J.-W. Wang, Z.-M. Zhang and T.-B. Lu, *Inorg. Chem.*, 2020, **59**, 6301–6307.
196 X. Song, Q. Guan, Z. Cheng and W. Li, *Appl. Catal., B*, 2018, **227**, 13–23.
197 M. Usman, A. Helal, M. M. Abdelnaby, A. M. Alloush, M. Zeama and Z. H. Yamani, *Chem. Rec.*, 2021, **21**, 1771–1791.
198 M. Liu, Y.-F. Mu, S. Yao, S. Guo, X.-W. Guo, Z.-M. Zhang and T.-B. Lu, *Appl. Catal., B*, 2019, **245**, 496–501.
199 G. E. Cmarik, M. Kim, S. M. Cohen and K. S. Walton, *Langmuir*, 2012, **28**, 15606–15613.
200 G. Wang, C.-T. He, R. Huang, J. Mao, D. Wang and Y. Li, *J. Am. Chem. Soc.*, 2020, **142**, 19339–19345.
201 M. Chu, Y. Li, X. Chen, G. Hou, Y. Zhou, H. Kang, W. Qin and X. Wu, *J. Mater. Chem. A*, 2022, **10**, 23666–23674.
202 Y.-C. Hao, L.-W. Chen, J. Li, Y. Guo, X. Su, M. Shu, Q. Zhang, W.-Y. Gao, S. Li, Z.-L. Yu, L. Gu, X. Feng, A.-X. Yin, R. Si, Y.-W. Zhang, B. Wang and C.-H. Yan, *Nat. Commun.*, 2021, **12**, 2682.